Numerical study of conjugate heat transfer in a continuously moving metal during solidification
by David Greif

A thesis submitted in partial fulfillment of the requirements for the degree of Master of Science in Mechanical Engineering
Montana State University

Abstract:
Heat transfer problems involving phase-changes have important applications in the field of engineering, such as metal casting, welding, wire drawing, optic fiber drawing,, fiber-glass drawing, and icing on airfoil surfaces. This study investigated the conjugate heat transfer in the continuous casting process. The investigated material was aluminum and it was assumed to be isotropic. The flow within the liquid phase was assumed to be laminar and incompressible. Problem geometry included a cooling mold to extract heat from the solidifying metal. The effects of casting speed, inlet temperature, and cooling rates in the mold and post-mold regions on the solidification process were studied. Casting speed was expressed as the Peclet number (Pe), and the cooling rates were expressed as Biot numbers (Bi). Radiation between the mold and the solidified aluminum was examined, and its effect on the solidification process was investigated.

Due to a moving phase-transition boundary, the governing equations describing a two-phase flow in a continuous casting process are non-linear. Inside the phase transition zone, the latent heat of fusion was absorbed into material's specific heat. Specific heat evaluation within the two-phase region was done using the average specific heat method. The governing equations were coupled, discretized using the Galerkin technique, and solved using the finite element method.

The results were plotted as: solidification front locations and shapes; velocity vector fields; temperature distributions along the outer surface and the centerline; isotherms throughout the domain; local heat fluxes; and total non-dimensional heat flux values. The plots were studied and conclusions drawn with respect to each casting parameter.

Numerical results indicate that the casting speed and the mold-cooling rate have the strongest effect on the slope and location of the solidification front. The inlet temperature does not affect the phase-transition slope. Radiation between the mold and the cast material has negligible effects on the solidification process. The post-mold cooling rate does not affect the solidification process within the mold, but it has a strong effect on the temperature distribution in the post-mold region and on the total heat flux. All casting parameters reflect in local and total heat flux values.

NUMERICAL STUDY OF CONJUGATE HEAT TRANSFER IN A CONTINUOUSLY MOVING METAL DURING SOLIDIFICATION

by
David Greif

A thesis submitted in partial fulfillment
of the requirements for the degree

of

Master of Science

in

Mechanical Engineering

MONTANA STATE UNIVERSITY – BOZEMAN
Bozeman, Montana

May 1998

APPROVAL

Of a thesis submitted by

David Greif

This thesis has been read by each member of the thesis committee and has been found satisfactory regarding content, English usage, format, citations, bibliographic style, and consistency, and is ready for submission to the College of Graduate Studies.

Dr. Ruhul Amin — Ruhul Amin (Signature) — 5/11/98 (Date)

Approved for the Department of Mechanical and Industrial Engineering

Dr. Vic Cundy — Vic A. S. (Signature) — 5/11/98 (Date)

Approved for the College of Graduate Studies

Dr. Joseph Fedock — Joseph J. Fedock (Signature) — 5/18/98 (Date)

STATEMENT OF PERMISSION TO USE

In presenting this thesis in partial fulfillment of the requirements for a Master's degree at Montana State University – Bozeman, I agree that the Library shall make it available to borrowers under rules of the Library.

If I have indicated my intention to copyright this thesis by including a copyright notice page, copying is allowable only for scholarly purposes, consistent with "fair use" as prescribed in the U. S. Copyright Law. Requests for permission for extended quotation from or reproduction of this thesis in whole or in parts may be granted only by the copyright holder.

Signature 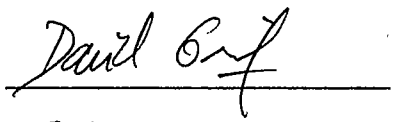

Date 5-18-1998

ACKNOWLEDGMENTS

I would like to thank Dr. Ruhul Amin for his guidance in my thesis work. I would like to express my appreciation to Dr. Alan George and Dr. Thomas Reihman for their work as committee members.

I would also like to thank the Sandia National Laboratories for the original version of the computer code used in this study, and to Dr. Ruhul Amin for the modified version which I used as a starting point in my thesis work.

This research was partially supported by the MONTS program, Montana State University's NSF/EPSCoR program. My appreciation is extended to the MONTS program, the Department of Mechanical and Industrial Engineering and to my mother Katarina Greif for providing me with financial assistance.

Finally, I would like to thank the staff of the Department of Mechanical and Industrial Engineering and my fellow graduate students, whose support made my work successful, enjoyable, and rewarding.

TABLE OF CONTENTS

TABLE OF CONTENTS - continued

LIST OF TABLES

LIST OF FIGURES

LIST OF FIGURES - continued

LIST OF FIGURES - continued

NOMENCLATURE

Symbol	Description
Ar	aspect ratio of cast material, L / W
Bi	Biot number - dimensionless convective heat transfer coefficient
Bi_1	pre-mold region Biot number
Bi_2	mold region Biot number
Bi_3	post-mold Biot number
C_l	specific heat of liquid-phase aluminum
C_r	ratio of specific heats, C_l/C_s
C_s	specific heat of solid-phase aluminum
d^u	discrete velocity convergence norm
d^T	discrete temperature convergence norm
g_y	acceleration due to gravity
h	dimensional convective heat transfer coefficient
h_r	dimensional radiative heat transfer coefficient
h_1	dimensional pre-mold convective heat transfer coefficient
h_2	dimensional mold region convective heat transfer coefficient
h_3	dimensional post-mold convective heat transfer coefficient
Gr	Grashof number
k	thermal conductivity
$k_{Al\text{-}s}$	thermal conductivity of solid aluminum
k_{Cu}	thermal conductivity of copper

NOMENCLATURE - continued

k_r	thermal conductivity ratio k_l / k_s
L	length of cast material
L_h	latent heat of fusion
L_1	length of pre-mold region
L_2	mold length
L_3	length of post-mold region
Nu	Nusselt number
P	pressure
Pe	Peclet number
q	local heat flux
q"	heat flux normal to the surface
Q	total dimensionless heat flux
Q_{av}	average dimensionless heat flux
Q^0	fitted dimensionless heat flux
r^2	variance in fitted model / variance of numerical data
Re	Reynolds number
Ste	Stefan number
t	time
t_{ml}	mold thickness
T	temperature
T_0	temperature at the inlet

NOMENCLATURE – continued

T_m	melting point temperature
T_s	solidification temperature for aluminum
T_∞	ambient temperature
u	x direction velocity component
U_0	withdrawal speed
v	y direction velocity component
W	half thickness of cast material

Greek Symbols

α	thermal diffusivity
β	coefficient of volumetric expansion
δ_{ij}	Dirac delta function
ΔT	half of the solidification temperature interval
ε_{Al}	emissivity of aluminum
ε_{Cu}	emissivity of copper
ε_P	penalty parameter in finite element formulation
μ	dynamic viscosity
ρ_l	density of liquid aluminum
ρ_s	density of solid aluminum
Θ	non-dimensional temperature
Θ_0	non-dimensional inlet temperature

NOMENCLATURE – continued

σ	Stefan Boltzman constant, 5.67E-8 $W/m^2 \cdot K^4$

Subscripts and Superscripts

av	average value
Al	aluminum
Cu	copper
l	liquid phase
m	property at melting point
ml	mold property
s	solid phase
0	condition at the inlet
∞	ambient value
*	non-dimensional quantity

ABSTRACT

Heat transfer problems involving phase-changes have important applications in the field of engineering, such as metal casting, welding, wire drawing, optic fiber drawing, fiber-glass drawing, and icing on airfoil surfaces. This study investigated the conjugate heat transfer in the continuous casting process. The investigated material was aluminum and it was assumed to be isotropic. The flow within the liquid phase was assumed to be laminar and incompressible. Problem geometry included a cooling mold to extract heat from the solidifying metal. The effects of casting speed, inlet temperature, and cooling rates in the mold and post-mold regions on the solidification process were studied. Casting speed was expressed as the Peclet number (Pe), and the cooling rates were expressed as Biot numbers (Bi). Radiation between the mold and the solidified aluminum was examined, and its effect on the solidification process was investigated.

Due to a moving phase-transition boundary, the governing equations describing a two-phase flow in a continuous casting process are non-linear. Inside the phase transition zone, the latent heat of fusion was absorbed into material's specific heat. Specific heat evaluation within the two-phase region was done using the average specific heat method. The governing equations were coupled, discretized using the Galerkin technique, and solved using the finite element method.

The results were plotted as: solidification front locations and shapes; velocity vector fields; temperature distributions along the outer surface and the centerline; isotherms throughout the domain; local heat fluxes; and total non-dimensional heat flux values. The plots were studied and conclusions drawn with respect to each casting parameter.

Numerical results indicate that the casting speed and the mold-cooling rate have the strongest effect on the slope and location of the solidification front. The inlet temperature does not affect the phase-transition slope. Radiation between the mold and the cast material has negligible effects on the solidification process. The post-mold cooling rate does not affect the solidification process within the mold, but it has a strong effect on the temperature distribution in the post-mold region and on the total heat flux. All casting parameters reflect in local and total heat flux values.

INTRODUCTION

Heat transfer problems involving melting and solidification represent an area of great practical importance in the field of engineering. Technology examples include metal casting, wire drawing, welding, anti-icing on airfoil surfaces, fiber-glass drawing, optic fiber drawing, and more.

Continuous casting is a commonly used phase change process in metal forming. The phase change problems are always non-linear, which is due to the moving boundary between the solid and the liquid phase, and have been approached analytically and numerically. Analytical techniques that have been developed to solve phase-change problems include the heat balance integral, Goodman (1958), variation technique, Yeh and Chung (1975), embedding, Boley (1974), isotherm migration, Crank and Gupta (1975), and source and sink methods, Keung (1980). Siegel (1984) used the Cauchy boundary value method to analytically solve the continuous casting problem. Analytical methods provide approximate solutions and have a common drawback; they result in very complicated mathematical formulations when solving multidimensional problems.

Two common ways to numerically model the process are to apply the finite element or finite difference methods. Both, the finite difference and finite element methods appear to be practical in solving the phase change problems.

In both methods, the solidification front position is determined during the analysis.

There are two different computational mesh variations commonly applied to the problem; one is the time-variant mesh, which traces the interface position; the second uses a fixed mesh technique. The fixed mesh approach is considerably simpler but has a drawback in dealing with non-linearity in material properties. The fixed mesh approach requires absorbing the latent heat into material's properties such as specific heat and enthalpy. While offering better results, the time variant mesh approach is limited to simple geometries.

The fixed mesh approach can be further divided into equivalent heat capacity and enthalpy models. An efficient finite difference approach using the equivalent heat capacity was developed by Hsiao (1985). Lee and Chiou (1995) modified Hsiao's (1985) results for the finite element method. In the present work Lee's method has been employed and will be discussed in more detail in the following sections.

Motivation for Present Research

The continuous casting process is an important production process in the metal forming industry. Most of the steel made every year is continuously cast. Therefore, much attention has been given to numerical modeling of the process, with the intention to improve and better understand the process. The cost of numerical modeling is considerably lower compared with experimental modeling in industry. For the same reasons there is extensive interest within the steel and metallurgy industry to fund such research projects and benefit from the results.

Continuous casting parameters greatly affect the quality of cast products. Typical parameters include the withdrawal velocity (velocity at which molten metal is withdrawn from the molten metal reservoir), amount of superheat (the temperature difference between the molten metal at the inlet and the solidification temperature), and the cooling rates in the mold and post-mold regions. These parameters affect the physics of the solidification process, including the solidification front position, solidification front slope, which directly reflect in the strength of the cast product, its uniformity and microstructure. Predicting these properties is highly desired in metallurgical industry, and was the motivation for numerical modeling of the process presented here.

The original computer program used in this research was provided by the Sandia National Laboratories, and was modified for a two-phase flow by Dr. Ruhul Amin at Montana State University. Its main limitation was with respect to the time step used to simulate a transient process. Temperature change at any

node over one time interval was not allowed to exceed the temperature interval over which solidification was expected to occur, as reported by Morgan et al. (1978). Lee and Chiou (1995) developed a method, which was insensitive to the temperature interval over which the solidification was expected to occur. The method allowed for use of larger time steps to save computing time. The time step used to simulate a transient process was found to have little effect on average and maximal errors.

Decreased computational complexity and maintained level of accuracy reported by Lee and Chiou (1995) were the motivation for the present work. As a part of the present work, the program was modified for use of the average specific heat model presented by Lee and Chiou (1995).

The essence of Lee and Chiou's (1995) technique is in applying the average specific heat method to evaluate the specific heat within the solidification interval. Although in present study the metal under consideration is pure aluminum and it solidifies at an exact temperature, the material was modeled to solidify over a temperature interval, in order to test the method. On that temperature interval an abrupt change in specific heat occurs, because of latent heat absorption into the material's specific heat. Details of this method are discussed later.

Problem Description

The concept of continuous casting is described next. A simplified continuous casting schematic is shown in Figure 1. The figure shows the cross-section of the planar two-dimensional geometry. Metal is heated above its melting point and thereafter withdrawn from the molten metal reservoir, commonly referred to as the tundish, at a constant withdrawal speed. Following the entry point is the cooling mold, where heated metal loses enough heat to form a solid shell. In the present study, the mold was modeled as solid copper and the outer mold-surfaces were cooled by forced convection. The solidified metal is further cooled in the sub-mold region, usually by forced convection. This is commonly done by water/air spray-cooling. The effects of the amount of superheat, varying withdrawal speed, and the heat transfer rates in the mold- and post-mold were investigated as a part of the project. In the present study of aluminum solidification process, the flow within the liquid phase was assumed to be laminar.

The main objective of the present research was to conduct a numerical study of the continuous casting process by applying the average specific heat method. The effects of convective heat transfer rates in the mold and post-mold regions, coupled with varying inlet temperature (amount of superheat) and withdrawal speed, were studied. The geometry of the model with basic linear dimensions is shown in Figure 2. Symmetric nature of the problem allowed us to consider only one half of the material.

The material studied is aluminum, and it was modeled as Newtonian incompressible fluid within the Boussinesq approximation. The flow is assumed to be laminar. This holds for the liquid phase. The solid phase is modeled as a fluid with a 'very large' viscosity as in the solid region, the kinematic viscosity approaches infinity.

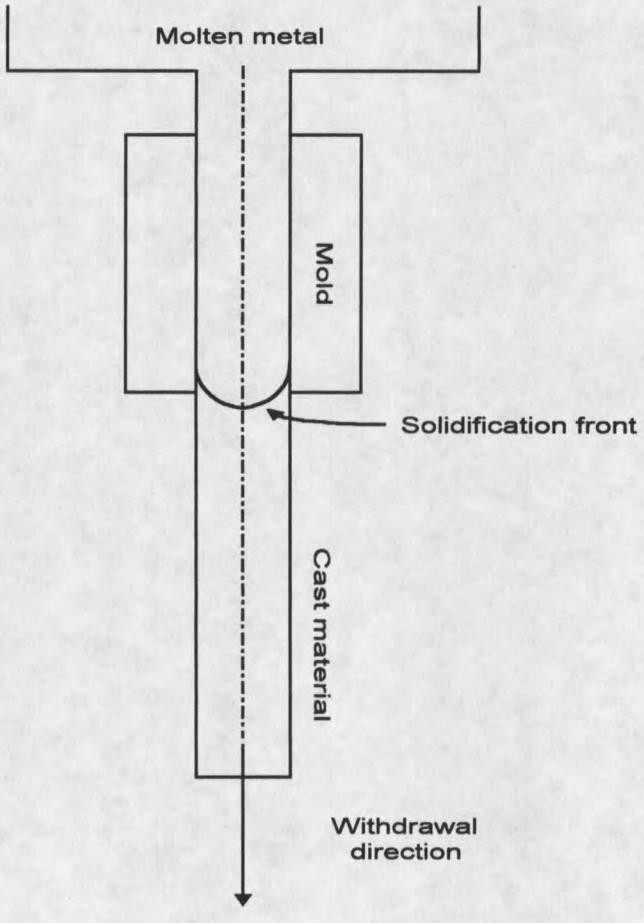

Figure 1. Schematic of a continuous casting process.

Figure 2 illustrates the basic geometry of the problem and it shows the partition of the problem domain into the pre-mold, mold and post-mold regions.

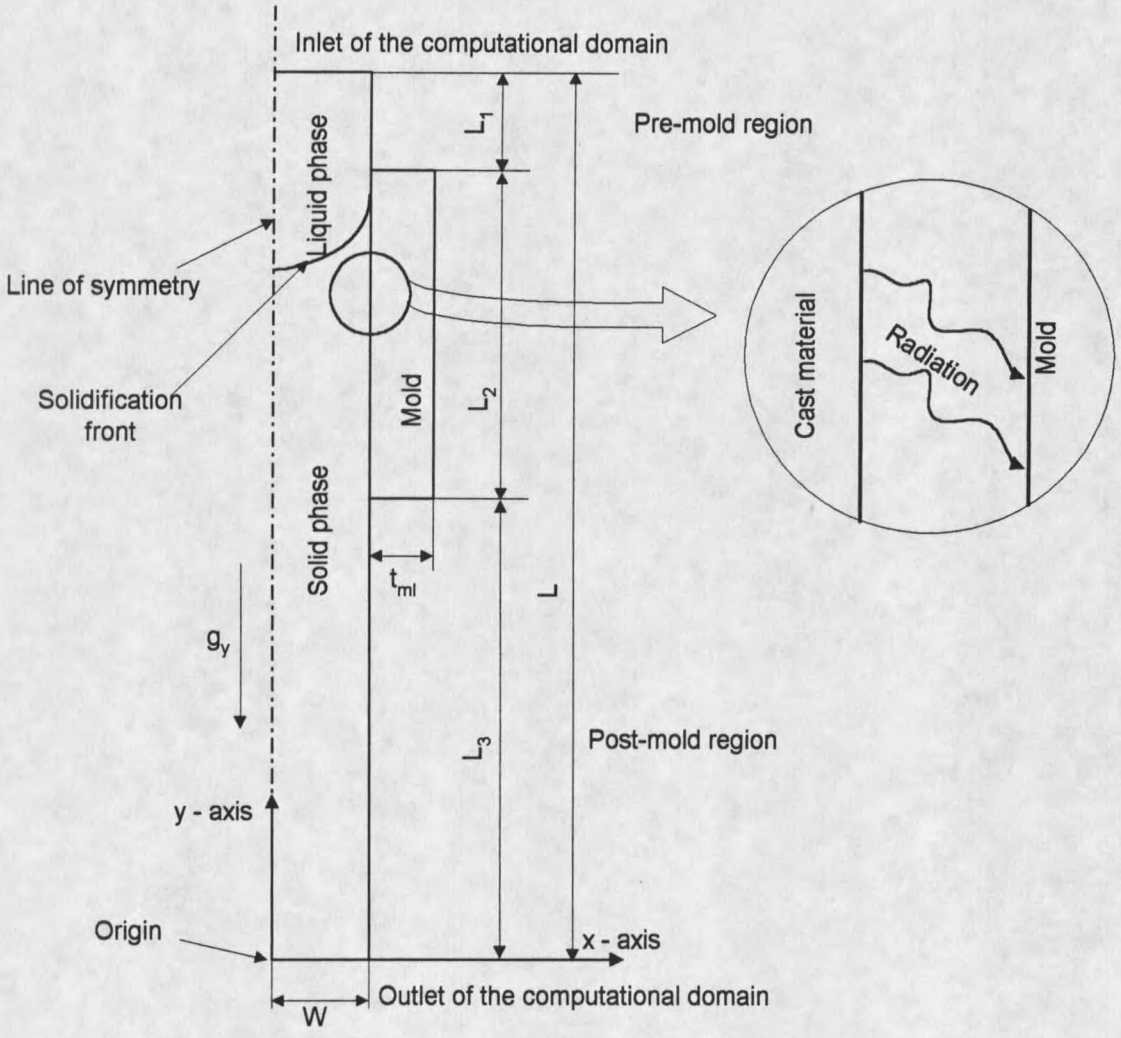

Figure 2. Schematic diagram of problem geometry.

According to the schematic presented in Figure 2, the aspect ratio for the problem was defined as

$$Ar = \frac{L}{W}. \qquad (1.1)$$

L is the length of the material, and W is the half thickness. Figure 2 shows that L_1 is the length of the pre-mold region, L_2 is the length of the mold, L_3 is the length of the post-mold region, and t_{ml} is the mold thickness.

The numerical investigation was performed using a finite-element code, originally known as 'NACHOS II'. The code was developed at the Sandia National Laboratories to solve single phase fluid mechanics and heat transfer problems. It was designed for the finite element analysis of steady-state or transient, two-dimensional, incompressible, viscous flows using the Galerkin technique. The program was then modified by Dr. Ruhul Amin at Montana State University to model two phase flows, including solidification problems. The present work is a further modification of the code and it is implemented using the average specific heat method presented by Lee and Chiou (1995).

The numerical simulations were carried out on a DEC "Alpha Server 2100 4/200" with 256 Mb of RAM.

Background

Starting in the late 1940's and continuing through the 90's, significant attention has been given to numerical modeling of the continuous casting process. Computer models turned out to be a relatively inexpensive way to predict this widely used manufacturing procedure. Several authors have approached the subject using different techniques.

The pioneering work dates back to 1940's when Eyres et al. (1946) investigated variable heat flow in the solids. Since then modeling the solidification systems numerically has been among major areas of research in the heat and mass transfer community.

Bonacina et al. (1973) presented numerical solutions to phase-change problems. The three-time level implicit scheme was unconditionally stable and convergent. The problem was defined as transient non-linear unsteady heat conduction problem. Their finite difference method was based on an analytical approach consisting of an approximation of the latent heat effect by a large heat capacity over a small temperature range. The method was capable of solving melting and solidification problems but was limited to problems with small temperature intervals over which the change of phase was expected to occur. They assumed pure conduction in the liquid phase. However, they remarked upon the possibility of an error when making such simplification.

An improved algorithm for heat conduction problems with a change of phase was presented by Morgan et al. (1978). They simplified and improved the

previously mentioned work by Bonacina et al. (1973). The objective was to reconsider the latent heat effect in a way such that the latent heat effect accompanied with a phase-change is approximated by integration of the terms involving the heat capacity. Therefore, an accurate evaluation of heat capacity is required at integrating points. In their method, quadratic iso-parametric elements were used and a very good level of accuracy was demonstrated. An important finding was that the time step size should be chosen so that the temperature change within one time interval should not exceed the temperature change over which the solidification was assumed to occur.

Gartling (1977) presented important work in computer modeling of convective heat transfer problems. Gartling's approach was applicable for both free and forced convection heat transfer and was based on a finite element method. The field equations were discretized using the Galerkin method. The solutions for the problems with temperature-dependent properties were presented. As mentioned before, Gartling's finite element computer program (NACHOS II) was used as the basis for the present work.

Siegel (1984) presented an analytical model of a continuously cast slab ignot. The model included an insulated mold following the molten metal entrance. He assumed the spatial variation of heating of the interface by the liquid phase to be a known function. In his two-region model, convection in the liquid was neglected and conduction was assumed to be the only mode of heat transfer. The heat flow was proposed to occur through the liquid metal to the solidification

interface and to the cooled ignot sides. By making these assumptions, a purely mathematical approach was taken in order to determine the solidification front position. The results were obtained by a Cauchy boundary value method, which was applied in two steps. First the interface shape was obtained to satisfy heat removal from the interface due to the latent heat of fusion and due to a generalized non-uniform heat transfer from the superheated metal. The second step was to obtain the heat conduction from the liquid metal to the solidification interface. Siegel stated that the shape of the interface is important in forming certain types of crystal structures.

An efficient algorithm for melting and solidification simulation was presented by Hsiao (1985). His finite difference method was capable of solving melting and solidification heat transfer problems. The latent heat of fusion was taken into account by using a linear interpolation of the nodal temperatures. The scheme was insensitive of the magnitude of the solidification interval, i.e., temperature range within which the solidification is expected to occur. Therefore, solidification of alloys, which solidify over an interval, and solidification of pure materials, which solidify at an exact temperature, can be modeled.

Thomas et al. (1990) presented a turbulent steel solidification model, which simulated the fluid flow inside a continuous slab-casting machine by applying the finite element method. Their work consisted of separate 2-D models for the nozzle and the mold region. Parameters under investigation were the velocity fields, effect of nozzle angle, casting speed, and turbulence simulation

parameters. The predicted flow patterns showed good agreement with the measured data. It was concluded that the overall flow field is relatively insensitive to process parameters.

Very important theoretical work in transport processes associated with continuously moving materials undergoing thermal processes was initially done by Jaluria (1992), and was very applicable to investigations of continuous casting process. The focus of Jaluria's research was on thermal buoyancy, transients, and forced flow in the ambient medium. Besides publishing the newly developed results, Jaluria also summarized and outlined previous achievements.

An important step forward in thermal modeling of the continuous casting process was the work by Kang and Jaluria (1993). They developed an enthalpy method, assuming a heat transfer coefficient at the surface of the material, to solve one dimensional two-zone problems and two-dimensional problems. In both cases the finite difference method was employed. The numerical results were found to follow the expected physical trends. For the small Peclet number range the effects of axial diffusion, the cooling rate inside the mold, the withdrawal speed, and the thermal buoyancy forces, were considered. The results were in good agreement with published analytical results. The interface shape and the resulting temperature field were found to be strongly dependent upon the cooling rate inside the mold and the withdrawal speed. Axial diffusion effects were found to be important and the effect of buoyancy forces to be insignificant for the parametric ranges considered. Their findings were also

applicable to other phase change processes involving moving materials, such as crystal growing, plastic extrusion, and glass fiber drawing.

Huang et al. (1992) investigated superheat dissipation in continuous casting machines. They developed a two-dimensional mathematical model to predict temperature and velocity fields within the liquid region. It was found that most of the heat is dissipated in the mold or just below the mold. Also, the amount of superheat and the casting speed were discovered to have a dominant effect on heat flux. Other parameters such as mold width, nozzle jet angle, and submergence depth, and their effects on the heat flux and the growth of shell were also investigated. Two-dimensional mathematical model predicted many three-dimensional results accurately.

Thomas (1993) presented the stress model of a casting process. Mathematical stress generation models are of great interest in the industry. Stress is modeled by coupled, transient heat transfer analysis including solidification, shrinkage, and fluid flow effects. Phenomena were further modeled by including phase transition, temperature, stress, plastic creep, mold distortion, and three-dimensional stress and crack formation. Because of high complexity the results had limited applicability when first presented. Recently due to highly increased computer capability and adequate mechanical property data, the results are getting more attention.

The modified latent heat method was presented by Lee and Tzong (1995) to properly model the latent heat effect in the solidification of a binary alloy. The

species and momentum equations were solved in the liquid and mushy zones. No species equation was needed in the solid phase because the eutectic state was imposed on the eutectic front – the front between the solid phase and mushy region. The mushy zone is the region between the solid and the liquid phase. To determine the mushy and the liquid zone interfaces, an interpolation technique was proposed. Good agreement with the experimental data was demonstrated.

An important aspect in the modeling of continuous casting has been researched and presented by Choudhury and Jaluria (1994). It has been found that convection in the post-mold region might have an important effect on the nature of solidification. The work was a continuation of Jaluria's (1992) publication. Forced convective heat transfer from a continuously moving heated cylindrical rod has been investigated in detail. The governing equations were elliptic and were solved employing a finite volume method. Heat transfer in the solid material was coupled with the heat transfer in the cooling liquid through the boundary conditions. The results of their study were very important in understanding and modeling the convective heat transfer in the post-mold region of the continuous casting process.

Further work on convective cooling of cylindrical surfaces was presented by Buckingham and Haji-Sheikh (1995). They investigated the cooling of high temperature cylindrical surfaces using a water/air spray. Two distinct regions were recognized in the post-mold region; radiation dominated, and convection-dominated regions. It was found that between the two regions there is a transition

region. Non linearity in convective heat transfer coefficient was discovered. The effects of droplet size and water content in the spray have been analyzed. The phenomena can be used as a guide to design better heat treating systems in metal forming processes.

Lee and Chiou (1995) presented a new multilevel finite element technique to solve phase change problems. The procedure proved to be very efficient for analyzing transient heat transfer with a change of phase. An average specific heat method was employed to simulate the properties of the elements undergoing the change of phase. In that region, an abrupt change of specific heat occurs due to latent heat absorption. An algorithm for analyses of heat transfer problems, including melting and solidification, was developed by Hsiao (1985). Lee and Chiou (1995) modified the algorithm for the use with the finite element method and achieved a very important improvement. The time step was found to have little effect on the average and maximum errors. Therefore, a larger time step can be used to save computing time. Also, the method was found to be insensitive of the temperature interval over which solidification is expected to occur.

Thomas and Ho (1996) presented a model of the continuous casting process developed using a spreadsheet program, Microsoft Excel, running on a personal computer. The model consisted of two-dimensional steady state finite difference heat conduction calculations within a mold, coupled with a one-dimensional solidification heat transfer of the solidifying shell. Model predictions

showed good agreement with previous solutions. It was found that spreadsheet programs running on personal computers are capable of solving relatively complex problems that would require extensive effort using conventional programming languages.

Currently extensive research is being done at the University of Illinois Urbana Champaign guided by Brian Thomas. Mathematical and numerical models were developed and emphasis is given to modeling of the steel-solidification process. Their research is focused on modeling the turbulent flow since the nature of the steel solidification process is highly turbulent. Many of their models include submerged-entry nozzle design. Other points of interest are stress generation, material shrinkage, determination of microstructure, and crack formation.

PROBLEM FORMULATION

Introduction

In the present study, the continuous casting process was assumed to be transient, two-dimensional, and laminar in the liquid portion of the flow. Viscosity in the solidified region was assumed to be 'very large' in order to model a solid material. The liquid portion was assumed to be a Newtonian fluid. The cooling mold was defined as a solid with constant material properties. The boundary conditions were set as described in Initial and Boundary Conditions section. Convection heat transfer coefficients in the pre-mold, mold and post-mold regions were taken as constants along the respective boundaries. Material density was assumed to be constant throughout each phase.

When metal solidifies during a continuous casting process, an interfacial gap forms between the mold and the cast metal, which results in a lower contact area between the mold and cast metal. Lower contact area results in a lower interfacial heat transfer coefficient, which was expected to influence the heat flux. Since an interfacial gap is formed, the radiation heat transfer was expected to have an impact on the heat flux. In the present work, the radiation between the mold and the material was taken into consideration, and was defined in a user-supplied subroutine.

The mold material was chosen to be copper. Specific heats for the solid and liquid regions were assumed to be constants. Specific heat at each node within the phase-change temperature interval was calculated using the average specific heat method developed by Lee and Chiou (1995). Details about specific heat evaluation using the average specific heat method will be described in the Numerical Method section.

As described earlier, the governing equations for the continuous casting problem were solved using a finite element method based on Galerkin technique. Sub-parametric quadrilateral nine-node elements were used to generate the finite element mesh. A nine-noded quadrilateral element is shown below in Figure 3.

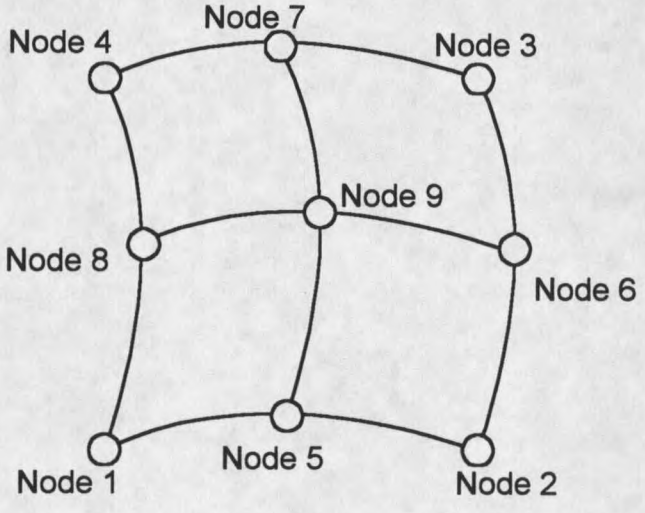

Figure 3. Typical 9-noded iso-parametric element.

Governing Equations

The present problem was concerned with the conjugate convective, conductive, and radiative heat transfer. Throughout the entire computational domain the conductive heat transfer was present. Along the outside mold surface and in the post-mold region, the mode of heat transfer was forced convection. Pre-mold region was assumed insulated. Radiative heat transfer takes place in the mold region beyond the phase transition front, where an interfacial air gap is formed.

The problem was described as planar and two – dimensional. The fluid was assumed to be Newtonian and incompressible within the Bossinesq approximation. The change in density upon the change of phase was assumed negligible. The flow within the liquid phase was assumed to be laminar. Materials were assumed to be homogenous and isotropic, i.e. material properties were independent of the coordinate direction. Material properties were temperature independent and were constant within each phase. The effect of latent heat was absorbed into the material's specific heat. Viscous dissipation was assumed to be negligibly small. Tensile stress effect in the liquid portion of the flow becomes an issue at higher withdrawal speeds, but it was neglected in the present study.

The flow was described by conservation laws for mass (continuity), momentum (Navier – Stokes), and by the energy equation. The basic equations describing the two-phase flow are given next.

The conservation of mass is enforced through the continuity equation. For constant density the equation is:

$$\frac{\partial u}{\partial x}+\frac{\partial v}{\partial y}=0 \tag{2.1}$$

Momentum equation in x and y directions respectively have the following forms:

$$\rho\frac{\partial u}{\partial t}+\rho u\frac{\partial u}{\partial x}+\rho v\frac{\partial u}{\partial y}=-\frac{\partial P}{\partial x}+\mu\left[\frac{\partial^2 u}{\partial x^2}+\frac{\partial^2 u}{\partial y^2}\right] \tag{2.2}$$

$$\rho\frac{\partial v}{\partial t}+\rho u\frac{\partial v}{\partial x}+\rho v\frac{\partial v}{\partial y}=-\frac{\partial P}{\partial y}+\mu\left[\frac{\partial^2 v}{\partial x^2}+\frac{\partial^2 v}{\partial y^2}\right]+\rho g_y\beta(T-T_\infty) \tag{2.3}$$

The energy equation is:

$$\rho C\left[\frac{\partial T}{\partial t}+u\frac{\partial T}{\partial x}+v\frac{\partial T}{\partial y}\right]=k\left[\frac{\partial^2 T}{\partial x^2}+\frac{\partial^2 T}{\partial y^2}\right] \tag{2.4}$$

Density, ρ, is constant throughout the solid and liquid phases. Specific heat, C, is constant in liquid (C_l) and solid (C_s) phases. Specific heat in the solidification region is evaluated according to the average specific heat method to accommodate for the latent heat removal. The approach is described later in a separate section. Thermal conductivity, k, is defined as follows:

$$\begin{aligned} k &= k_s && for\, T < T_s-\Delta T \\ k &= k_s+\frac{k_l-k_s}{2\Delta T}\left[T-(T-\Delta T)\right] && for\, T_s-\Delta T \le T \le T_s+\Delta T \\ k &= k_l && for\, T > T_s+\Delta T \end{aligned} \tag{2.5}$$

In equation (2.5) T_s is the solidification temperature for aluminum. ΔT represents a half of the temperature interval over which solidification was modeled to occur.

Equations (2.1) through (2.4) together with the boundary conditions, which are discussed next, form a complete set for determination of velocity, temperature fields in both, liquid and solid phases, and velocity fields in the liquid region. In the liquid region momentum equation is coupled with the energy equation and the mass conservation equation (continuity) to obtain the solution fields. In the solid region a very high value of viscosity is assigned. Momentum equations become very stiff. Thereby the momentum and continuity equations are eliminated from the problem. The only remaining governing equation in the solid phase is the energy equation. Within the solid phase the velocity component parallel to the withdrawal direction is assigned the magnitude of the withdrawal speed, U_0, and the other velocity component equals zero.

Initial and Boundary Conditions

Table 1 lists the boundary conditions in dimensional form. Dimensions correspond to the schematic given in Figure 2.

Table 1. Boundary conditions in dimensional form.

BC Type	Dimensional Location
$u = 0$	$x = 0,\ 0 \le y \le L$
	$x = W,\ 0 < y < L$
	$0 \le x \le W,\ y = 0$
	$0 \le x \le W,\ y = L$
$v = -U_0$	$0 \le x \le W,\ y = 0$
	$0 \le x \le W,\ y = L$
$\partial T/\partial y = 0$	$0 \le x \le W,\ y = 0$
$\partial T/\partial x = 0$	$x = 0,\ 0 \le y \le L$
$h_1 = 0$	$x = W,\ L_2 + L_3 \le y \le L$
h_2	$W \le x \le W + t_{ml},\ y = L_3$
	$x = W + t_{ml},\ L_3 \le y \le L_2 + L_3$
	$W \le x \le W + t_{ml},\ y = L_2 + L_3$
h_3	$x = W,\ 0 \le y \le L_3$

Note that x=0 defines the centerline of the material, x = W defines the outside edge, y=0 defines the outlet of the computational domain, y = L defines the inlet plane, and t_{ml} denotes the mold thickness, as defined in Figure2. L_1, L_2, L_3 are also defined in Figure 2. In this study, $L_1 = 0.1 \cdot L$, $L_2 = 0.4 \cdot L$, $L_3 = 0.5 \cdot L$.

As discussed earlier, the radiation heat transfer between the mold and the solidified metal was taken into account through the boundary condition. The mold/metal interfacial heat transfer was accounted for by applying a radiative heat transfer coefficient at the metal/mold interface. It is defined as:

$$h_r = \frac{\sigma(T_{Cu}^2 + T_{Al}^2)(T_{Cu} + T_{Al})}{\frac{1}{\varepsilon_{Al}} + \frac{1}{\varepsilon_{Cu}} - 1} \qquad (2.6)$$

In equation (2.6), the subscript '*Cu*' represents the considered property at the inside surface of the cooling mold, and the subscript '*Al*' represents the considered property at the outer surface of the cast material in the solidified region. σ is the Stefan-Boltzman constant. ε is the material's emissivity and was assumed constant along the respective boundaries.

As mentioned in the earlier section, the investigated metal was aluminum and it was modeled as a Newtonian fluid. The cooling mold material was solid copper. Thermophysical properties for all materials used in numerical modeling of the continuous casting process are listed in Table 2.

Table 2. Thermophysical properties for aluminum and copper.

Property	Liquid Al	Solid Al	Copper	Units
Density, ρ	2542.5	2542.5	8933	kg/m^3
Specific heat, C	1080	1076	385	J/kg·K
Viscosity, μ	$1.3x10^{-3}$	10^{10}	---	kg/m·s
Thermal conductivity, k	94.03	238	401	W/m·K
Thermal expansion, β	$1.2x10^{-4}$	---	---	1/K
Latent heat of fusion, L_h	$3.95x10^5$	---	---	J/kg
Phase change temperature	936.52	930.52	---	K
Emissivity, ε	---	0.3	0.5	---

Normalization of Governing Equations

The following non-dimensional variables were introduced in order to normalize the governing equations:

$$x^* = \frac{x}{W} \tag{2.7}$$

$$y^* = \frac{y}{W} \tag{2.8}$$

$$u^* = \frac{u}{U_0},\ v^* = \frac{v}{U_0} \tag{2.9}$$

$$P^* = \frac{P}{\rho \cdot U_0^2} \tag{2.10}$$

$$\Theta = \frac{T - T_\infty}{T_s - T_\infty} \tag{2.11}$$

$$t^* = \frac{t \cdot U_0}{W} \tag{2.12}$$

In the above expressions x and y are linear dimensions, u and v are the velocity components, U_0 is the withdrawal velocity, W is the half thickness of the cast material, and was chosen as the characteristic length. Superscript '*' represents the dimensionless counterparts for the dimensional variables. T_∞ is the surrounding temperature calculated from the definition of the Stefan number given in equation (2.20).

By substituting the above dimensionless parameters into dimensional governing equations (2.1), (2.2), (2.3), (2.4), the normalized governing equations are obtained.

$$\frac{\partial u^*}{\partial x^*}+\frac{\partial v^*}{\partial y^*}=0 \tag{2.13}$$

$$\frac{\partial u^*}{\partial t^*}+u*\frac{\partial u^*}{\partial x^*}+v^*\frac{\partial u^*}{\partial y^*}=\frac{-\partial P^*}{\partial x^*}+\frac{1}{\mathrm{Re}}\left(\frac{\partial^2 u^*}{\partial x^{*2}}+\frac{\partial^2 u^*}{\partial y^{*2}}\right) \tag{2.14}$$

$$\frac{\partial v^*}{\partial t^*}+u*\frac{\partial v^*}{\partial x^*}+v^*\frac{\partial v^*}{\partial y^*}=\frac{-\partial P^*}{\partial y^*}+\frac{1}{\mathrm{Re}}\left(\frac{\partial^2 v^*}{\partial x^{*2}}+\frac{\partial^2 v^*}{\partial y^{*2}}\right)+\frac{Gr}{\mathrm{Re}^2}\Theta \tag{2.15}$$

$$\frac{\partial \Theta}{\partial t^*}+u^*\frac{\partial \Theta}{\partial x^*}+v^*\frac{\partial \Theta}{\partial y^*}=\frac{1}{Pe}\left(\frac{\partial^2 \Theta}{\partial x^{*2}}+\frac{\partial^2 \Theta}{\partial y^{*2}}\right) \tag{2.16}$$

After non-dimensionalizing the material's specific heat, the Stefan number appeared in non-dimensional form of the material's heat capacity. Details about the average specific heat method are discussed in detail in a separate section. At this point it is sufficient to recognize that four criteria define the specific heat at the nodes within the solidification interval. In all definitions, terms including the latent heat, L_h, are expressed in terms of Stefan number, *Ste*. A general procedure is illustrated next.

As shown in Hsiao (1985), the specific heat at a node undergoing phase transition can be written as:

$$C = a(T)\cdot\left(\frac{L_h}{2\cdot\Delta T} + f(T, C_s, C_l)\right) \tag{2.17}$$

In equation (2.17), *'a'* and *'f'* represent functions of temperature and specific heats for solid and liquid regions. *'a'* and *'f'* vary for each case, as described later, and only a general procedure is illustrated here for reasons of brevity.

Specific heat is non-dimensonalized with the solid-phase specific heat, C_s.

$$C^* = a'(\Theta)\cdot\left(\frac{f'(\Theta)}{Ste} + f''(\Theta, C_r)\right) \tag{2.18}$$

where C_r is the ratio of specific heats defined as

$$C_r = \frac{C_l}{C_s} \tag{2.19}$$

Functions *a'*, *f'*, and *f''* in equation (2.18) will change for different criteria that define the specific heat inside the solidification interval and are discussed in detail in the Average Specific Heat section. Non-dimensional parameters appearing in the normalized governing equations are defined as:

$$\mathrm{Re} = \frac{U_0 W \rho}{\mu} \qquad \mathrm{Pr} = \frac{\mu\cdot C}{k} \qquad Gr = \frac{g_y \beta \rho^2 \cdot W^3 (T - T_\infty)}{\mu^2}$$

$$Pe = \mathrm{Re}\cdot\mathrm{Pr} \qquad Ste = \frac{C_s(T_s - T_\infty)}{L_h} \tag{2.20}$$

Non-dimensional Boundary Conditions

The normalized boundary conditions are listed in Table 3.

Table 3. Normalized boundary conditions.

BC Type	Non-dimensional Location
$u^* = 0$	$x^* = 0,\ 0 \le y^* \le L / W$
	$x^* = 1,\ 0 < y^* < L / W$
	$0 \le x^* \le 1,\ y^* = 0$
	$0 \le x^* \le 1,\ y^* = L / W$
$v^* = -1$	$0 \le x^* \le 1,\ y^* = 0$
	$0 \le x^* \le 1,\ y^* = L / W$
$\partial\Theta/\partial y^* = 0$	$0 \le x^* \le 1,\ y^* = 0$
$\partial\Theta/\partial x^* = 0$	$x^* = 0,\ 0 < y^* < L / W$
$Bi_1 = 0$	$x^* = 1,\ (L_2 + L_3) / W \le y^* \le L / W$
Bi_2	$1 \le x^* \le 1 + t_{ml} / W,\ y^* = L_3 / W$
	$x^* = 1 + t_{ml} / W,\ L_3 / W \le y^* \le (L_2 + L_3) / W$
	$1 \le x^* \le 1 + t_{ml} / W,\ y^* = (L_2 + L_3) / W$
Bi_3	$x^* = 1,\ 0 \le y^* \le L_3 / W$

In this study $t_{ml} / W = 0.25$, $L / W = 20$, $L_1 / W = 2$, $L_2 / W = 8$, $L_3 / W = 10$.

NUMERICAL METHOD

Introduction

To obtain solutions for most realistic boundary value problems approximate solution methods are most commonly considered. Most popular numerical solution methods are in general divided into two groups – finite element methods (FEM) and finite difference methods (FDM). Both methods have the same objective, namely to reduce the infinite number of degrees of freedom. In the present work, a continuous problem described by a set of partial differential equation was reduced to a discrete problem (finite number of degrees of freedom) described by a system of algebraic equations. Although the results of both methods are very similar, the procedures are sufficiently different. In the present work the finite element method was used to solve the continuous casting problem. Basic concepts are described in this chapter. Detail discussion on this can be found in Gartling (1987).

A computational mesh was chosen as fixed with time, and is described next. The computational matrix describing the ranges of parameters used for the current study is shown later.

Finite Element Formulation

The modeling procedure begins with the division of some continuous regions of interest into a number of simply shaped regions called finite elements. As mentioned above, the elements were chosen as fixed in space. Within an element, dependent variables (u_i, P, T) are interpolated in terms of values to be determined at a set of nodal points. In order to determine the equations for these nodal point unknowns, an individual element is separated from the global system.

Within each element, velocities, pressure, and temperature are approximated as:

$$u_i(x_i,t) = \Phi^T(x_i)u_i(t) \tag{3.1}$$
$$P(x_i,t) = \Psi^T(x_i)P(t) \tag{3.2}$$
$$T(x_i,t) = \Theta^T(x_i)T(t) \tag{3.3}$$

where u_i, P, T are element nodal point unknowns, and Φ, Ψ, Θ are vectors of interpolation functions. The above approximations are substituted into the field equations and yield a set of functional equations.

Conservation of momentum:

$$f_{u1}(\Phi,\Psi,\Theta,u_i,P,T) = R_{u1} \tag{3.4}$$
$$f_{u2}(\Phi,\Psi,\Theta,u_i,P,T) = R_{u2} \tag{3.5}$$

Incompressibility or mass conservation:

$$f_P(\Phi,u_i) = R_P \tag{3.6}$$

Energy conservation equation:

$$f_T(\Phi,\Theta,u_i,T) = R_T \tag{3.7}$$

R's in the above equations denote residual errors resulting from approximations given in equations (3.1, 3.2,3.3). In order to reduce these errors to zero, the Galerkin form of method of weighted residuals is used. That is achieved by making the residuals orthogonal to the interpolation functions over each element as indicated below,

$$\langle \Phi, f_{u1} \rangle = \langle \Phi, R_{u1} \rangle = 0 \tag{3.8}$$
$$\langle \Phi, f_{u2} \rangle = \langle \Phi, R_{u2} \rangle = 0 \tag{3.9}$$
$$\langle \Psi, f_P \rangle = \langle \Psi, R_P \rangle = 0 \tag{3.10}$$
$$\langle \Theta, f_T \rangle = \langle \Theta, R_T \rangle = 0 \tag{3.11}$$

where <a,b> denotes the inner product and is defined as

$$\langle a,b \rangle = \int_{\Omega} a \cdot b d\Omega. \tag{3.12}$$

Ω in equation (3.12) represents the area under consideration. Details in evaluating integrals defined in equation (3.12) are available in Gartling (1987).

The finite element method can be divided into the mixed FEM and the penalty FEM. In the mixed method, all of the dependent variables are directly approximated and retained in the global matrix problem. In the penalty method, which was used in the present work, pressure is eliminated from the matrix

problem and the overall size of the problem is thereby reduced. The following compressibility condition is considered:

$$\frac{\partial u_i}{\partial x_i} = -\varepsilon_P \cdot P \tag{3.13}$$

In the above expression, ε_P is the penalty parameter and is typically a small constant. Solutions of usual momentum equations converge to the solution of the real incompressible problem as ε_P approaches zero. Equation (3.13) can be used in the continuity equation. Galerkin method of weighted residuals produces the following:

$$GR^T U = -\varepsilon_P \cdot M_P P. \tag{3.14}$$

$$M\dot{U} + AC(U)U + K_P U + K(U,T)U + B(T)T = F(T); K_P = \frac{1}{\varepsilon_P} GR \cdot M_P^{-1} GR^T \tag{3.15}$$

This expression can be solved for pressure and substituted into the discretized form of the momentum equation. Therefore, the matrix problem description becomes:

$$\begin{bmatrix} M, 0 \\ 0, N \end{bmatrix} \begin{Bmatrix} \dot{U} \\ \dot{T} \end{Bmatrix} + \begin{bmatrix} AC(U) + K_P + K(U,T), B(T) \\ 0, \qquad\qquad D(U) + L(T) \end{bmatrix} \begin{Bmatrix} U \\ T \end{Bmatrix} = \begin{Bmatrix} F(T) \\ G(T,U) \end{Bmatrix}. \tag{3.16}$$

The matrix equation (3.16) is a discretized form of the conservation equations for an individual finite element. AC and D matrices represent the advection of momentum and energy respectively; K and L represent diffusion of momentum and energy respectively. GR matrix is a gradient operator and GR^T is the divergence operator. Also note that pressure has been eliminated from the matrix problem. M and N matrices are the mass and capacitance terms in the field equations, and B matrix represents the buoyancy force. Importantly buoyancy force becomes irrelevant in the case of forced convection. Pressure can be recovered from equation (3.17) using the known velocity as indicated

$$P = -\frac{1}{\varepsilon_P} M_P^{-1} GR^T U. \tag{3.17}$$

Average Specific Heat Method

The adjusted specific heat method was originally developed by Hsiao (1985) for the finite difference method. The approach was capable of incorporating the latent heat of fusion into the material's heat capacity for cases when solidification occurs at a certain temperature (pure metal solidification), or over a temperature range (binary alloys). It was assumed that the specific heat at a certain node is dependent on the four adjacent nodes. Figure 4 shows the combined specific heat including the latent heat effect over the solidification interval $2\Delta T$. T_m in Figure 4 represents the melting temperature.

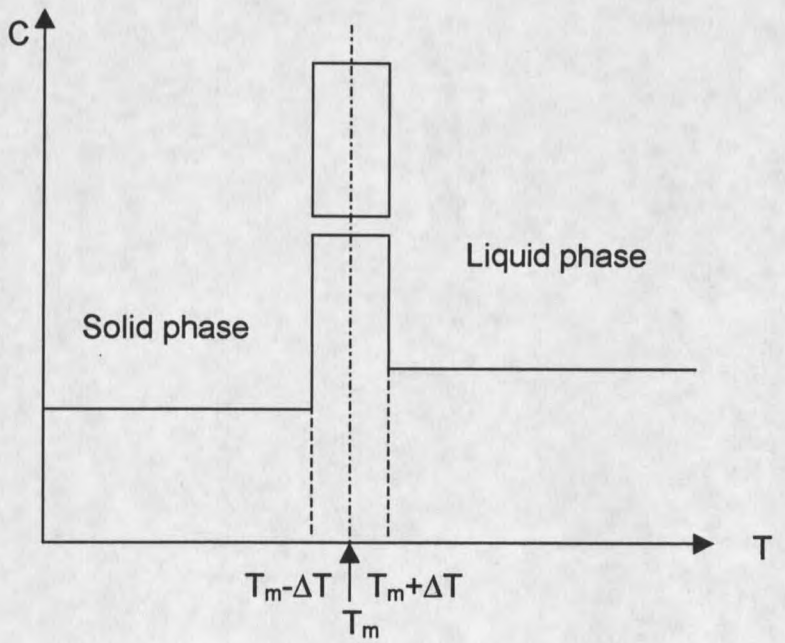

Figure 4. Latent heat effect on material's heat capacity.

To illustrate the computation of the adjusted specific heat at a node let us consider two nodes at temperatures T_1 and T_2, assuming that one of the two is inside the solidification region and $T_1 > T_2$. Hsiao (1985) discretized the material within T_1 and T_2 into solid, liquid, and molten. Adjusted specific heat, $C(T_1, T_2)$ at a node was calculated according to the following criteria:

$$If\ T_2 < T_1 < T_m - \Delta T$$
$$C(T_1, T_2) = C_s \tag{3.18}$$

$$If\ T_m + \Delta T < T_2 < T_1$$
$$C(T_1, T_2) = C_l \tag{3.19}$$

$$If\ T_2 < T_m - \Delta T\ and\ T_1 > T_m + \Delta T$$
$$C(T_1, T_2) = \frac{1}{(T_1 - T_2)}\left[2\Delta T\left(\frac{L_h}{2\Delta T} + \frac{C_s + C_l}{2}\right) + C_s \cdot (T_m - \Delta T - T_2) + C_l \cdot (T_1 - T_m - \Delta T)\right] \tag{3.20}$$

$$If\ T_m - \Delta T < T_2 < T_1 < T_m + \Delta T$$
$$C(T_1, T_2) = \frac{L_h}{2\Delta T} + \frac{C_s + C_l}{2} \tag{3.21}$$

$$If\ T_2 < T_m - \Delta T\ and\ T_m - \Delta T < T_1 < T_m + \Delta T$$
$$C(T_1, T_2) = \frac{1}{(T_1 - T_2)}\left[\left(\frac{L_h}{2\Delta T} + \frac{C_s + C_l}{2}\right)(T_1 - T_m + \Delta T) + C_s \cdot (T_m - \Delta T - T_2)\right] \tag{3.22}$$

$$If\ T_m - \Delta T < T_2 < T_m + \Delta T\ and\ T_m + \Delta T < T_1$$
$$C(T_1, T_2) = \frac{1}{(T_1 - T_2)}\left[\left(\frac{L_h}{2\Delta T} + \frac{C_s + C_l}{2}\right)(\Delta T + T_m - T_2) + C_l \cdot (T_1 - T_m - \Delta T)\right] \tag{3.23}$$

$$If\ 2\Delta T = 0$$
$$C(T_1, T_2) = \frac{1}{(T_1 - T_2)}\left[L_h + C_s \cdot (T_m - T_2) + C_l \cdot (T_1 - T_m)\right] \tag{3.24}$$

From Hsiao's (1985) results, Lee and Chiou (1995) developed an algorithm for use with finite element methods and it was applied in the present work. In the solid and liquid regions specific heat was again evaluated straightforwardly as C_s and C_l respectively, since they are not temperature dependent. For the elements undergoing phase transition, the nodes in the two-phase zone were reconsidered. Heat capacity at any node within the freezing interval depended not only on the four adjacent nodes, but also on its four corner nodes. Figure 5 shows a typical portion of a finite element mesh.

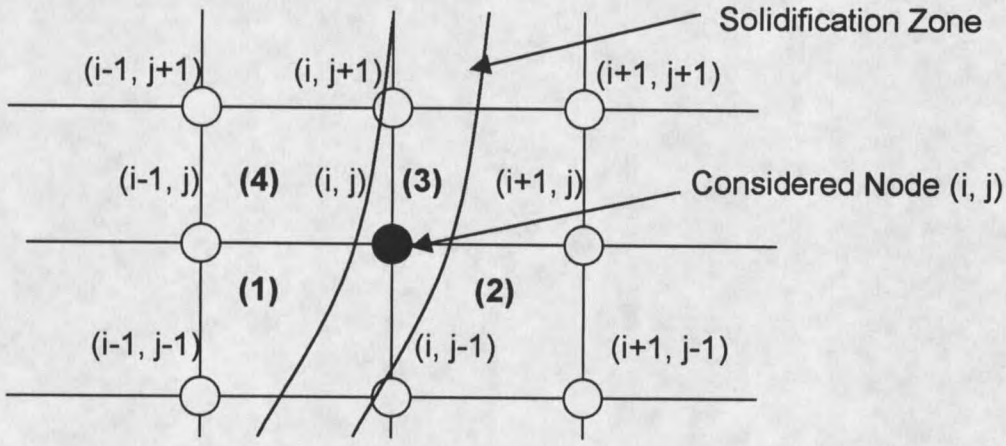

Figure 5. Typical portion of the finite element mesh.

As reported by Lee and Chiou (1995), specific heat at a node undergoing phase change can be expressed as follows,

$$C(T_{i,j}) = \frac{1}{4}\left[C_1(T_{i,j}, T_{av,1}) + C_2(T_{i,j}, T_{av,2}) + C_3(T_{i,j}, T_{av,3}) + C_4(T_{i,j}, T_{av,4})\right] \quad (3.25)$$

where

$$T_{av,i} = \frac{1}{4}(T_{1n} + T_{2n} + T_{3n} + T_{4n}) \quad (3.26)$$

As illustrated in Figure 5, each node has four adjacent sub-elements. T_{1n}, T_{2n}, T_{3n}, and T_{4n} in equation (3.26) are the nodal temperatures of four-noded sub-elements, and $T_{av,i}$ is the average temperature of the i^{th} adjacent sub-element. After the average temperature is determined for a sub-element under consideration, T_1 and T_2 values are assigned so that $T_1 > T_2$ for use in equations (3.18 - 3.24). Thereafter the adjusted specific heat, $C(T_{i,j}, T_{av,j})$, is calculated for that sub-element according to equations (3.18 - 3.24). The procedure is repeated for each sub-element and the average specific heat is finally calculated according to equation (3.25).

The method was found to be insensitive of the freezing temperature interval and of the time step used to simulate a transient process. Therefore larger time step can be used to decrease the computational time.

Computational Mesh

The computational mesh was chosen so that accurate results can be obtained and the computational time is minimized. The total computational time increases with the increase in the number of elements. The following is an overview of the mesh refinement test.

The finite element grids were arranged so that more elements were placed in the mold region and along the outside boundary of the cast metal. The reason were steeper temperature and velocity gradients in those regions.

It is important to clarify the convergence criteria used in the present work. NACHOS II uses the discrete norms to check for convergence. The norms are defined below.

$$d_{n+1}^{u_i} = \frac{1}{u_{i,\max}} \left(\sum_{j=1}^{N} \left(u_{i,j}^{n+1} - u_{i,j}^{n} \right)^2 \right)^{1/2}$$

$$d_{n+1}^{T} = \frac{1}{T_{\max}} \left(\sum_{j=1}^{N} \left(T_{j}^{n+1} - T_{j}^{n} \right)^2 \right)^{1/2} \qquad (3.20)$$

Subscript *max* represents the maximum value of a variable at the $(n+1)^{th}$ (current) time step, and *n* is the previous time step. When the norms decreased below the specified convergence criteria, the solution fields were considered to be at steady state. The convergence parameter in the present work was set to 10^{-6}.

For mesh sensitivity testing a grid with 320 elements (Mesh A) was chosen as the base for comparison. The number of elements was first doubled in

the mold region, resulting in the geometry with 400 elements (Mesh B). Finally, the number of elements was doubled throughout the entire domain, resulting in 640 elements (Mesh C). Four cases were run for the grid independence test. The ranges of the parameters are shown in Table 4. It is important to note here that the mold region (y*=17-20) was modeled as an insulated mold through the boundary condition (Bi_2 = 0). There was no pre-mold region. Along the outer edge surface of the post mold region (x* = d, y* = 0 - 17), a constant temperature boundary condition (Θ = 0) was applied.

Table 4. Computational matrix for grid independence test.

	Bi_2	Θ_0	Pe / Ste
Test 1	0	1.1	0.4
Test 2	0	1.5	0.4
Test 3	0	2.0	0.4
Test 4	0	1.5	1.0

Figure 6 shows the three computational grids (mesh A – 320 elements, mesh B – 400 elements, mesh C – 640 elements), for which the results were compared. Results are presented in Figures 7 and 8. Figure 7 shows the temperature along the outer edge for all three meshes. The plotted domain for the outer edge is the mold region only (y* = 17 - 20). The reason is that in the post mold region (y* = 0 - 17), the temperature boundary condition was applied and the temperature equaled the ambient temperature (Θ = 0).

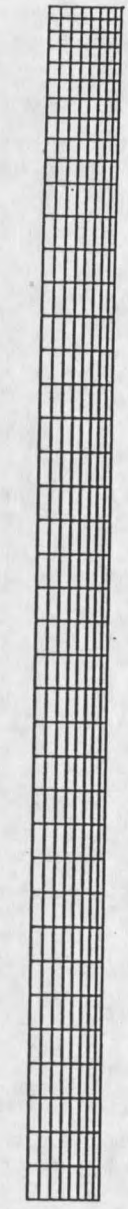

Mesh A

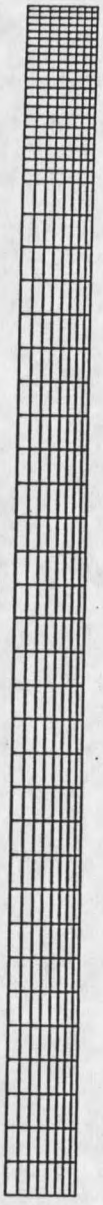

Mesh B

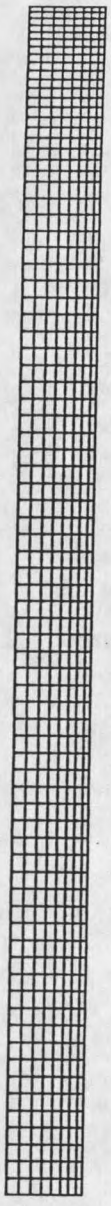

Mesh C

Figure 6. Meshes with 320, 400, and 640 elements.

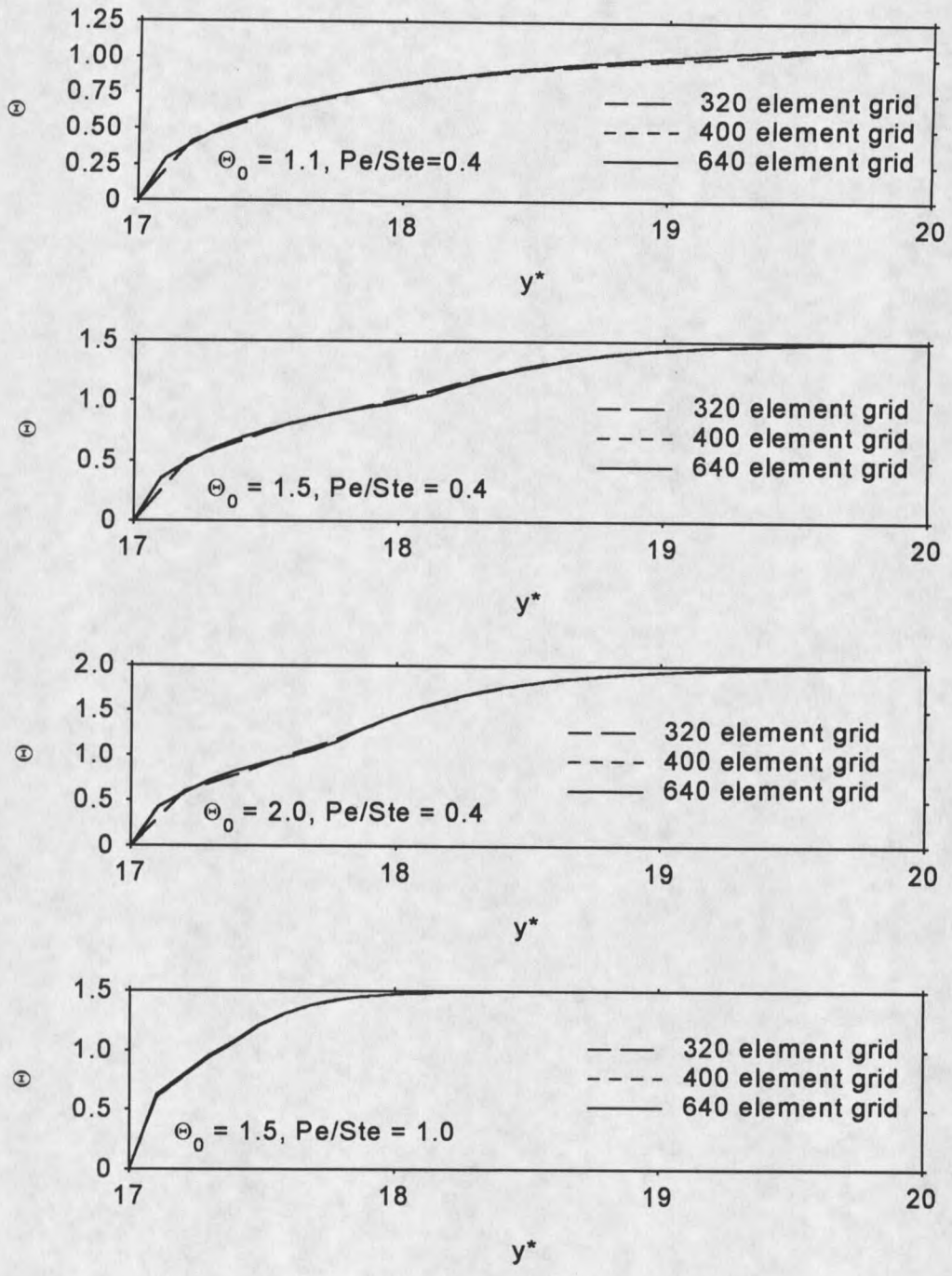

Figure 7. Mesh independence results – outer edge temperature.

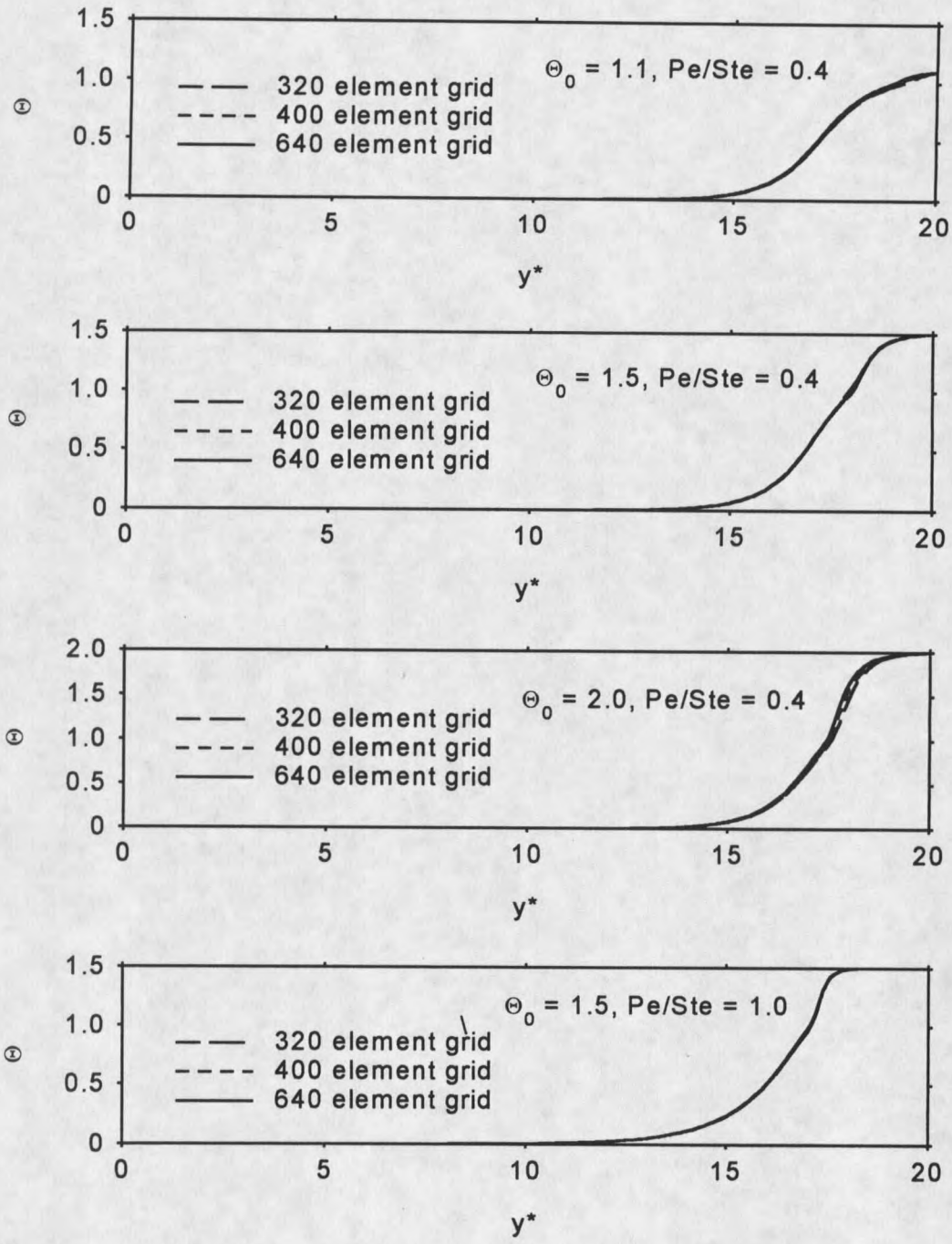

Figure 8. Mesh independence results – centerline temperature.

Figure 8 shows the temperature profiles along the centerline of the material. Plotted domain is for the entire computational domain length (y*=0 - 20).

Table 5. Mesh refinement test.

Mesh	Number of Elements	Number of Nodes	Max. % difference in average temperature, Θ_{av}	Computational time / iteration
A	320	1377	N/A	117 sec.
B	400	1717	1.6	153 sec.
C	640	2737	3	221 sec

The average temperatures were calculated along the respective boundaries by numerical integration. Mesh independence tests indicate that the grid consisting of 320 elements provides accurate results. Comparing the results for meshes A and B, the computational time increased by approximately 31%. The maximum average temperature difference occurred along the centerline and it was equal to 1.6% (Θ_0 = 1.5, Pe/Ste = 0.4).

When comparing meshes A and C, the maximum difference in average temperature increased to 3% (Θ_0 = 2.0, Pe/Ste = 0.4), and the computational time increased by 89%.

For the above reasons, the geometry consisting of 320 elements was chosen, i.e. the cast metal portion of the problem consisted of 320 elements.

Therefore, the grid spacing described by mesh A was used for the numerical computations in this research. Following the grid spacing of mesh A, a total of 374 elements were used for the geometry with the mold. This resulted in a total of 1617 nodes for the geometry of our computational domain, which is shown in Figure 9.

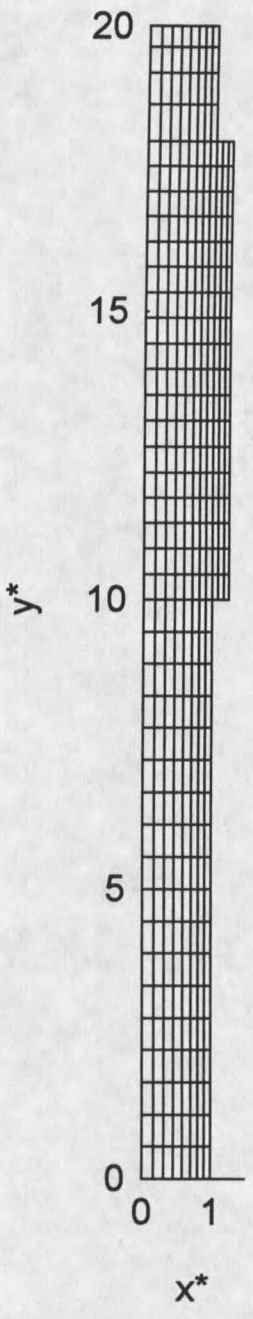

Figure 9. Computational domain with 374 elements.

Code Validation

To further establish the accuracy of the current computational method, results for selected cases obtained by the present technique were verified with other published results. Once the accuracy of the method was established, computations were extended for the cases for which no previous studies have been conducted.

The validation of the method presented in this work was done by running four cases, and comparing the results with the analytical solutions presented by Siegel (1984), who developed a mathematical model for the continuous casting process. The subject of comparison with Siegel (1984), were the solidification front locations.

The average specific heat method presented by Lee and Chiou (1995) was applied as discussed earlier, and solidification was modeled to occur over a temperature interval. Latent heat of fusion was absorbed into material's specific heat, as described in an earlier section. In dimensional terms aluminum solidifies at 933.52 K. The solidification temperature interval was assumed to be 930.52 – 936.52 K.

The input parameters for this study were the same as the ones for mesh independence tests shown in Table 4 earlier in this chapter. Withdrawal speed parameter (*Pe/Ste)* was varied from 0.4 to 1, and the superheat parameter (Θ_0) was varied from 1.1 to 1.5. Results are shown in Figure 10.

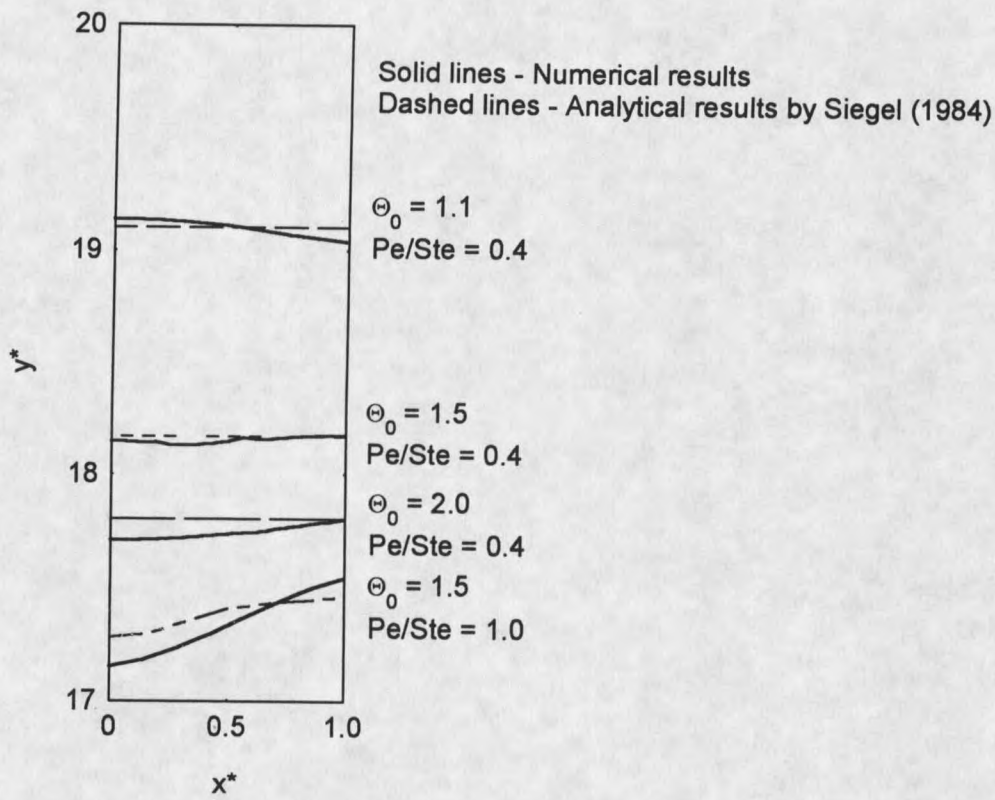

Figure 10. Comparison with the analytical results of Siegel (1984);

Pe/Ste = 0.4, 1.0, Θ_0 = 1.1, 1.5, 2.0.

Note that in Figure 9, the dashed lines represent the analytical results obtained by Siegel (1984), and the solid lines represent the numerical results.

For lower withdrawal speed conditions a very good agreement with analytical results was demonstrated. As the value of Pe/Ste increases, the agreement is not quite as good, which is due to Siegel's assumption that the withdrawal speed is low and that convective effects can be neglected compared with conduction effects. A similar observation was made by Kang and Jaluria

(1993) who compared the results of the enthalpy method with Siegel's analytical solutions. Overall good agreement with the published results was demonstrated. This gave confidence about the accuracy of the current numerical method.

Computational Matrix

Several cases were run to determine the effect of mold and post-mold cooling rates coupled with different withdrawal speeds and inlet temperatures. Four input parameters were varied; the mold heat transfer coefficient, Bi_2, post-mold heat transfer coefficient, Bi_3, inlet temperature, Θ_0, and withdrawal speed, *Pe*. In present research the Stefan number, *Ste*, was fixed at 2.5.

Specific interests of the current research were to determine the total heat flux from the cast metal, percentage of heat extracted in the mold, the solidification front location and its shape, and temperature distribution throughout the domain. The ranges of parameters used in this study were:

- Pe = 1 - 3.45
- Θ_0 = 1.2 - 2.7
- Bi_2 = 0.0249 - 0.0748
- Bi_3 = 0.042 - 0.1261.

For high values of *Pe,* numerical instability was discovered. Computational matrix showing the ranges of parameters used in the current study is shown in Table 5. A total of 50 cases were run for the current study, including the mesh refinement tests and the code verification runs.

Table 6. Computational matrix for the current study.

Pe	Θ_0	Bi_2	Bi_3	Number of Cases
1.2	1.2	0.0249, 0.0499, 0.0748	0.042	3
1.2	1.2	0.0249, 0.0499, 0.0748	0.084	3
1.2	1.2	0.0249, 0.0499, 0.0748	0.1261	3
1.5	1.2	0.0249, 0.0499, 0.0748	0.042	3
1.5	1.2	0.0249, 0.0499, 0.0748	0.084	3
1.5	1.2	0.0249, 0.0499, 0.0748	0.1261	3
1.5	1.5	0.0748	0.1261	1
1.5	2	0.0748	0.1261	1
1.5	2.5	0.0748	0.1261	1
1.5	2.7	0.0748	0.1261	1
1.0	1.2	0.0748	0.1261	1
1.35	1.2	0.0748	0.1261	1
1.65	1.2	0.0748	0.1261	1
1.8	1.2	0.0748	0.1261	1
2.0	1.2	0.0748	0.1261	1
2.15	1.2	0.0748	0.1261	1
2.3	1.2	0.0748	0.1261	1
2.5	1.2	0.0748	0.1261	1
3.45	1.2	0.0748	0.1261	1
2.5	1.2	0.0249	0.1261	1

Table 6 cont.

Pe	Θ_0	Bi_2	Bi_3	Number of Cases
2	1.2	0.0249	0.042	1
2.3	1.2	0.0249	0.042	1
2.5	1.2	0.0249	0.042	1
2.5	1.2,1.5,2.0	0.0748	0.1261	3

RESULTS AND DISCUSSION

Introduction

The numerical results presented in this chapter were obtained using a modified version of a finite element computer program called NACHOS II. Accuracy of the code was tested by comparing the results with the analytical solutions, reported by Siegel (1984). Mesh sensitivity tests were carried out to ensure that the chosen mesh provides accurate results within an acceptable computational time.

As discussed earlier, the working metal was chosen to be aluminum, and the flow in the liquid portion was assumed laminar and incompressible. Aluminum was chosen because it has not been modeled as extensively as steel. Studies involving steel solidification were presented by Thomas et al. (1990), Thomas (1993), Huang et al. (1992), Choudhary and Mazumdar (1995), De Santis and Ferretti (1996), Braun et al. (1996), to mention the most recent ones.

Published aluminum solidification studies are not nearly as common and include Peclet numbers lower than 1, Kang and Jaluria (1993). The present work is focused on the Peclet number range from 1.2 – 3.45 to explore the higher casting speed conditions, which are desired for reasons of productivity.

The effect of radiation heat transfer between the mold and the solidified metal during the solidification process was investigated. This aspect has not been studied in aluminum solidification modeling before.

As discussed in an earlier section, the objective of the current study was to investigate the heat transfer in the mold and post-mold regions. Also, of interest were the solidification front position and its shape, as functions of the withdrawal speed, amount of superheat, and the cooling rates in the mold and post-mold regions. For simplified conditions, a correlation between the total heat flux and the withdrawal speed was obtained. A similar correlation between the superheat and the heat flux was obtained as well. Temperature distributions along the outside surface and along the centerline of the cast material were investigated. Such findings are of practical importance in industry in order to predict the physics of the solidification process and to increase the productivity.

In the present study, the aspect ratio defined in equation (1.1) was Ar = 20.

Non-dimensionalizing the Results

The computer code used for the present work solves the governing equations and the boundary conditions in primitive variables. The input parameters need to be in dimensional form. Therefore, the results were expressed in dimensional form as well. However, for generality, the results are reported in non-dimensional form. Results are reported after steady state condition was achieved for each case. The following non-dimensional parameters were utilized to present the results.

The amount of superheat was defined as:

$$\Theta_0 = \frac{T_0 - T_\infty}{T_s - T_\infty} \tag{4.1}$$

In the above equation, T_∞ is the surrounding media temperature and was calculated from the definition of the Stefan number.

$$Ste = \frac{C_s \cdot (T_s - T_\infty)}{L_h} \tag{2.20}$$

Withdrawal speed was expressed as the Peclet number, in terms of the withdrawal speed, material's half thickness, and the thermal diffusivity.

$$Pe = \frac{U_0 \cdot W}{\alpha_s} \tag{4.2}$$

Convective heat transfer coefficients were expressed as the Biot numbers, *Bi*, and were defined for the mold region and for the post-mold region. The pre- mold region was assumed to be insulated, which makes the Biot

number equal to zero for that region. Biot numbers for the mold, Bi_2, and post mold regions, Bi_3, are expressed as:

$$Bi_2 = \frac{h_2 \cdot W}{k_{Cu}} \tag{4.3}$$

$$Bi_3 = \frac{h_3 \cdot W}{k_{Al-s}} \tag{4.4}$$

Local dimensional heat flux values at the outer boundary of the material were computed. Local dimensional heat flux, q'', was converted into the local dimensionless heat flux, $q^{*''}$, and thereafter numerically integrated using the Simpson's rule in order to obtain the average dimensionless heat flux, Q. The procedure is outlined below.

First, let us consider the energy balance at the outside edge of the material. The heat flux at that boundary can be expressed as

$$q'' = h \cdot (T - T_\infty) = -k \cdot \frac{\partial T}{\partial x} \tag{4.5}$$

where q'' is dimensional heat flux normal to the outer boundary. Dividing equation (4.5) by $k\,(T-T_\infty)\,/\,L$ results in the following form of the energy balance:

$$q^{*''} = \frac{q'' \cdot L}{k \cdot (T - T_\infty)} = \frac{h \cdot L}{k} \tag{4.6}$$

It is important to note here that the thermal conductivity in the above equation, k, is not constant throughout the domain. However, it is constant for

each phase. Local heat fluxes were finally integrated to obtain the average dimensionless heat flux, Q, for the entire outside surface.

$$Q = \int_0^1 q^{*''} \cdot dy^* \tag{4.7}$$

The above non-dimensional parameters permit generalization of the results. It should be noted at this point that while conducting the parametric study, not more than one input parameter was varied to allow for realistic comparison and meaningful interpretation of the results.

Four input parameters were varied to meet the objectives of the study. These parameters are withdrawal speed (*Pe*), amount of superheat (Θ_0), and mold and post-mold convective heat transfer coefficients (Bi_2 and Bi_3).

Effects of Withdrawal Speed

The withdrawal speed in non-dimensional form was expressed as the Peclet number, *Pe*. Several cases were run over a range of Peclet numbers keeping the amount of superheat constant. Two different cooling rates were investigated. Two sets of numerical results were obtained for the following input data:

- $\Theta_0 = 1.2$; $Bi_2 = 0.0249$; $Bi_3 = 0.042$; Pe = 1.2, 1.5, 2.0, 2.5
- $\Theta_0 = 1.2$; $Bi_2 = 0.0748$; $Bi_3 = 0.1261$; Pe = 1.2, 1.5, 2.0, 2.5, 3.45

The solidification front positions for these cases are shown in Figure 11. A practical point of interest in modeling the continuous casting process are the breakout conditions, i.e. conditions at which the solidification front moves beyond the mold. According to Huang et al. (1992), a maximum safe casting speed likely exists for each superheat at the given cooling conditions.

In cases when the solidification front moves past the mold exit, breakout would occur. For the second set of runs (high cooling rate: $Bi_2 = 0.0748$; $Bi_3 = 0.1261$) breakout conditions were not attained. This can be seen in Figure 11(b) where solidification fronts do not move beyond the mold region. Breakout is reached when the cooling rates are decreased, which can be seen in Figure 11(a). For the cases when the cooling rate was high ($Bi_2 = 0.0748$, $Bi_3 = 0.1261$), the Peclet number needed to be increased beyond the point when the computation became numerically unstable. This was found for the cases with the

Peclet numbers greater than 3.45. This finding suggests that for each cooling rate there is a limiting Peclet number that can be used to obtain a numerically stable solution, using the current method. Beyond this Peclet number, the flow in the liquid region becomes turbulent and the current method fails. The Reynolds number, *Re*, was computed for those cases and it was found that *Re* nears 10^3 as the Peclet number is increased beyond 3.45. The Reynolds number range from 10^3 to 10^4 is a transition region in which laminar flow assumptions cannot be applied with certainty.

Figure 12 shows the velocity field in the liquid region for different withdrawal speeds. The plots correspond to the cases plotted in Figure 11(b) and demonstrate good agreement with the solidification front locations. The vectors at the inlet ($y^* = 20$) are uniform due to the boundary condition. The length of the vectors at the inlet is the same for different values of *Pe* because the velocity was non-dimensionalized with the withdrawal speed, U_0, as shown in equation (2.9). As the metal cools down and approaches the solidification front, the size of the vectors decreases and eventually reaches zero at the solidification line. Closer to the solid/liquid interface the vector field tends to become less uniform, which is true for all withdrawal speeds. The vectors along the outer wall ($x^* = 1$) equal to zero due to the no-slip boundary condition in the liquid portion of the flow. The Reynolds number for these cases ranges from 203 – 583, indicating that laminar flow assumptions still apply.

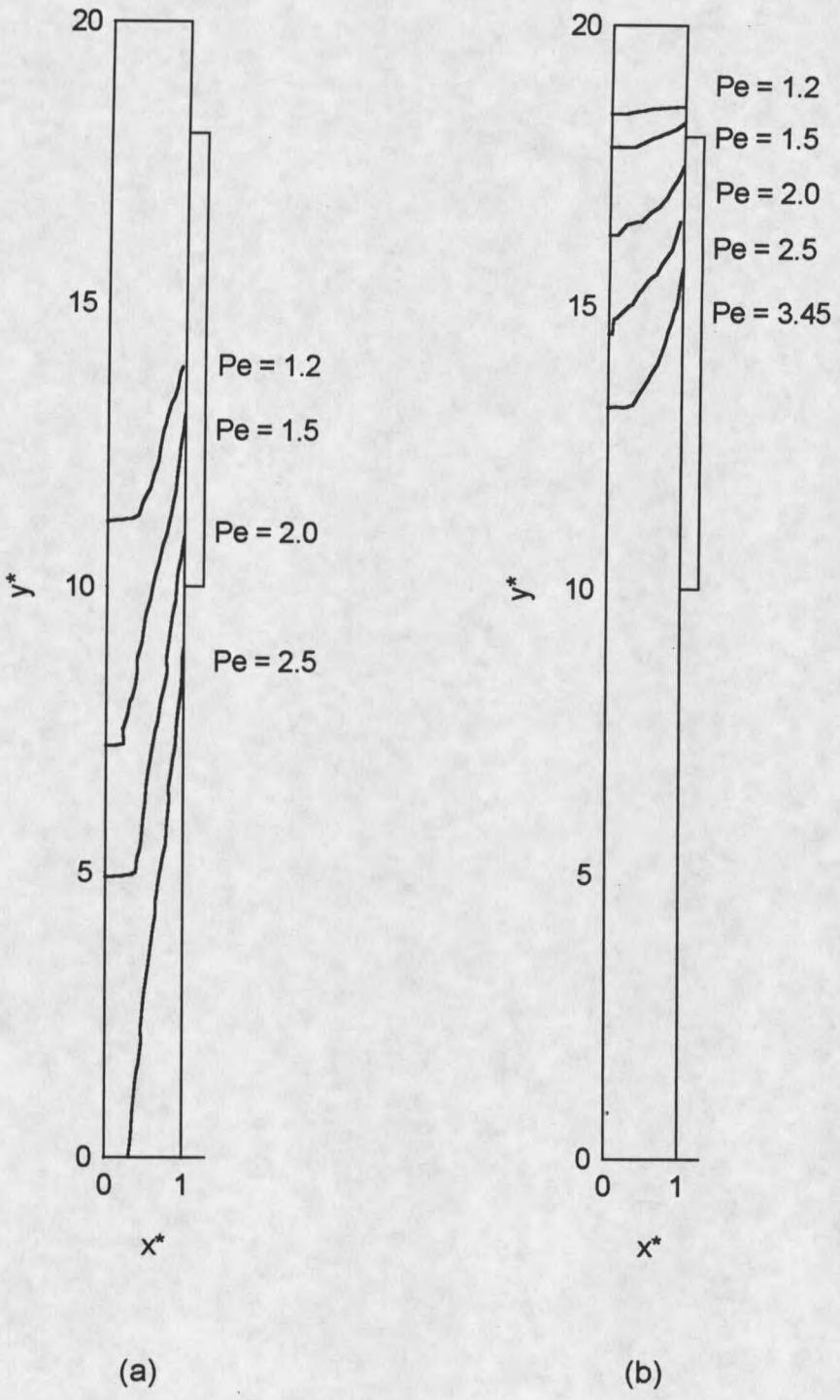

Figure 11. Effect of withdrawal speed; (a) $\Theta_0 = 1.2$, $Bi_2 = 0.0249$, $Bi_3 = 0.042$,

(b) $\Theta_0 = 1.2$, $Bi_2 = 0.0748$, $Bi_3 = 0.1261$.

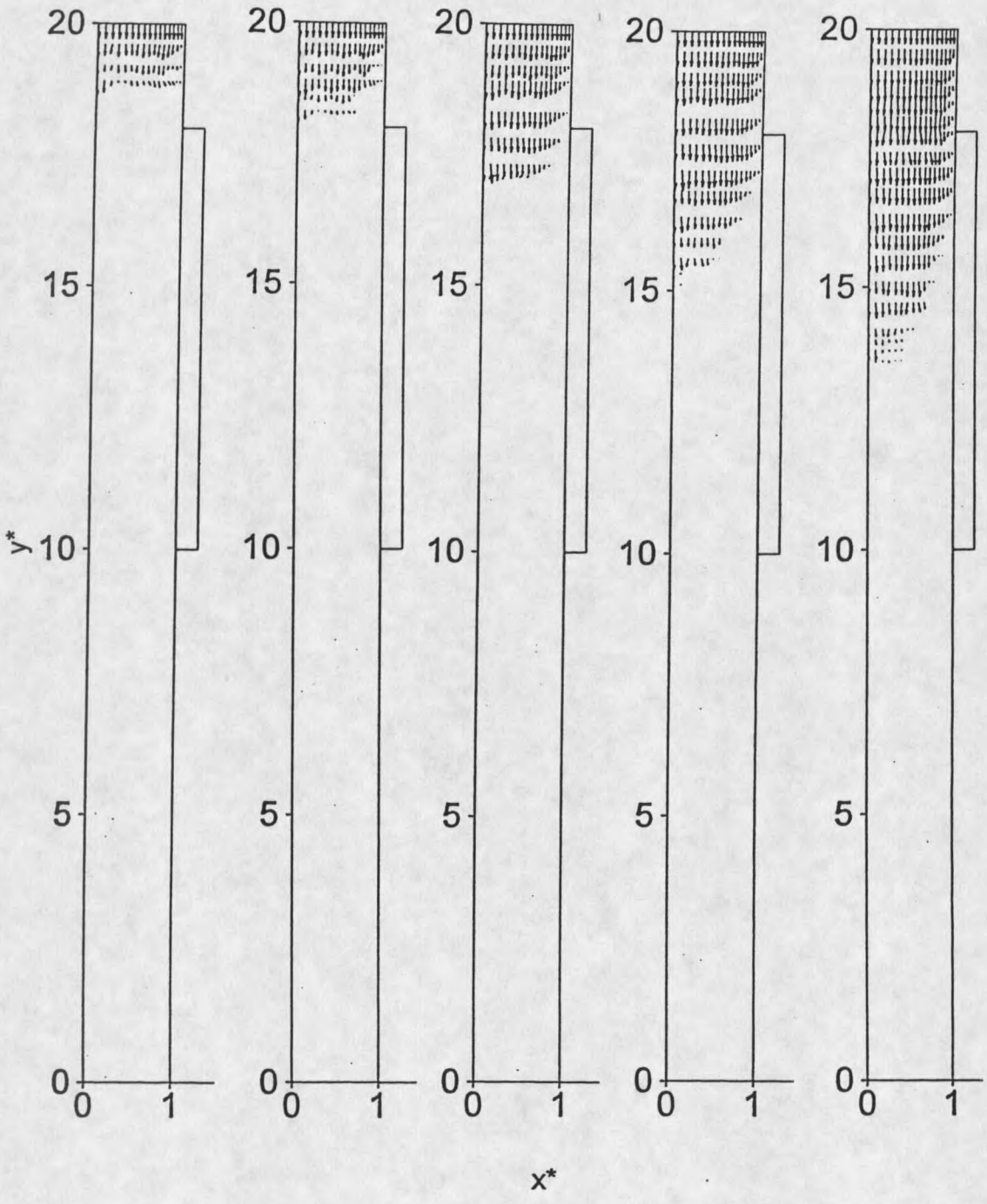

(a) Pe=1.2 (b) Pe=1.5 (c) Pe=2.0 (d) Pe=2.5 (e) Pe=3.45

Figure 12. Velocity vector field. Θ_0=1.2, Bi_2 = 0.0748, Bi_3 =0.1261,

Pe = 1.2, 1.5, 2.0, 2.5, 3.45.

Results presented in Figures 11 and 12 indicate that there is a direct relation between the Peclet number and the solidification front position. For higher values of *Pe*, the solidification front moved further down in the withdrawal direction, which holds true regardless of the other input parameters.

The Peclet number also influenced the slope of the solidification front. With increasing withdrawal speed, the slope of the front became steeper. For the liquid phase along the outer edge of the cast metal, the velocity equaled zero due to the boundary condition, regardless of the casting parameters. With increasing withdrawal speed, the maximum velocity increased. Considering this, the slope of the solidification front had to increase for high Peclet numbers.

The temperature distribution along the centerline and along the outside edge of the cast material offered another meaningful comparison. Temperatures along those lines were related to the casting speed. As the solidification front moved downstream, the superheated metal spread further downstream, which moved more heat further down by convection. Therefore the temperatures along the respective planes were expected to increase with the increasing Peclet number. Figure 13 shows the outside edge temperature profiles for the cases presented in Figure 11.

The outer edge temperatures show that the Peclet number had a visible effect on the temperature distribution in the pre-mold region ($y^* = 18 - 20$), where no convective heat transfer occurred ($Bi_1 = 0$). The effect is more obvious when *Pe* is low and Bi_2 is high (Figure 13(b)). Since the pre-mold region was

insulated, there was no heat leaving the surface, and the heat flow had to occur in the axial direction. The axial conduction effect in the pre-mold region was stronger for cases with high cooling rates and low withdrawal speeds. The axial heat conduction influenced the temperature field in the pre-mold region (near the mold entrance), and resulted in a temperature decrease near the mold entrance.

Figure 14 shows the centerline temperature distribution for the same group of cases. When considering the pre-mold centerline temperatures for different values of *Pe*, the same effect of axial conduction was observed as along the outer edge. The case for Pe=2.5 in Figure 11(a) shows that the solidification front along the centerline was beyond the end of the computational domain. Figure 14(a) is in agreement with that, since the temperature never dropped below the solidus temperature ($\Theta = 1$).

When observing Figures 13(a) and 14(a) (low cooling rate, $Bi_2 = 0.0249$, $Bi_3 = 0.042$) we notice a slope change after the material entered the mold region ($y^*<18$). This is due to the convective heat transfer in that region. For cases when Pe=1.2, 1.5, 2.0, the curves became flat at the point where solidification occurs ($y^*\sim15$ and lower). These locations indicate the region where the latent heat was absorbed. This was concluded knowing that the temperature remains constant during latent heat removal. For higher withdrawal speed, this region was stretched out.

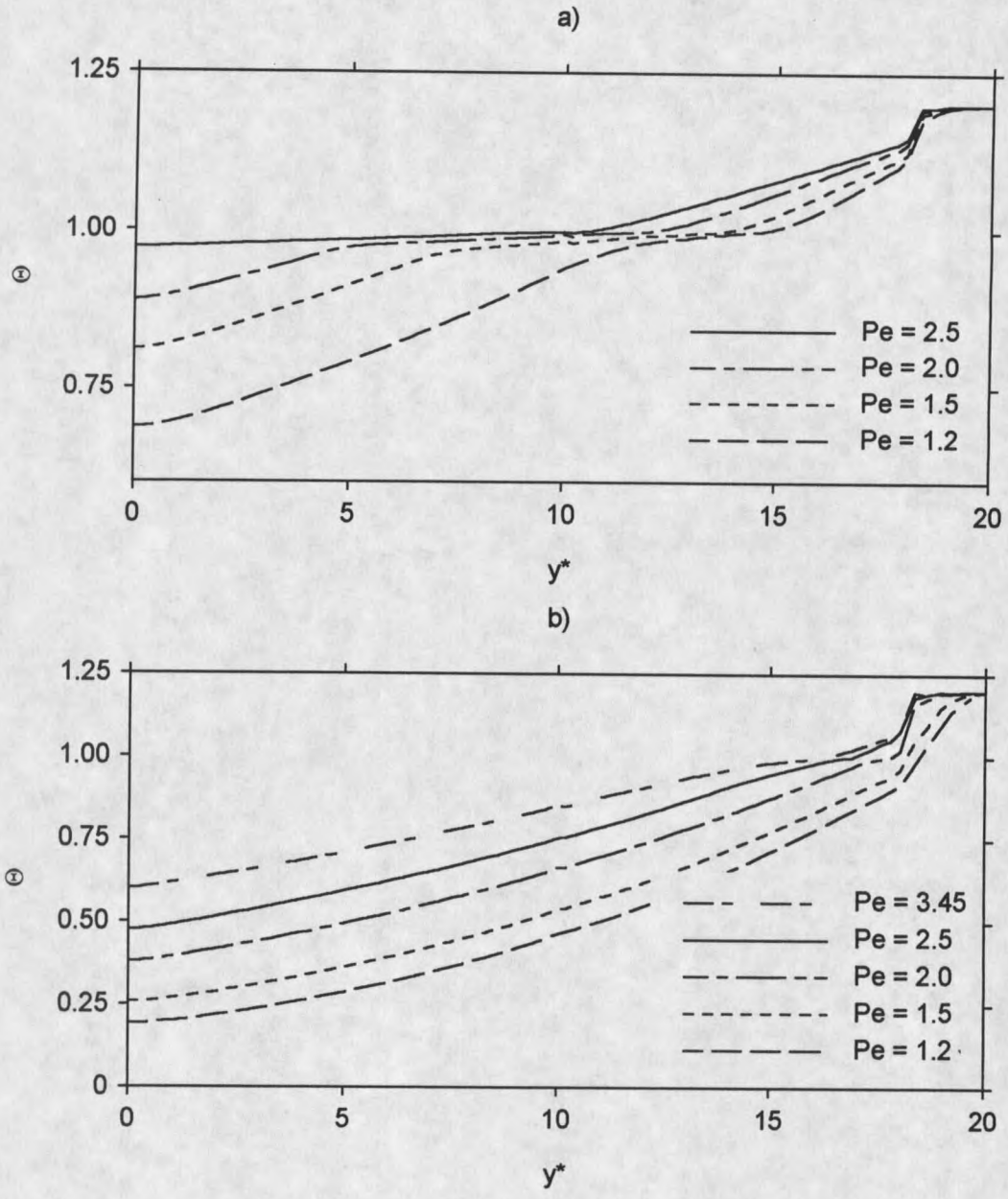

Figure 13. Outside edge temperature for (a) $Bi_2 = 0.0249$, $Bi_3 = 0.042$;

(b) $Bi_2 = 0.0748$, $Bi_3 = 0.1261$.

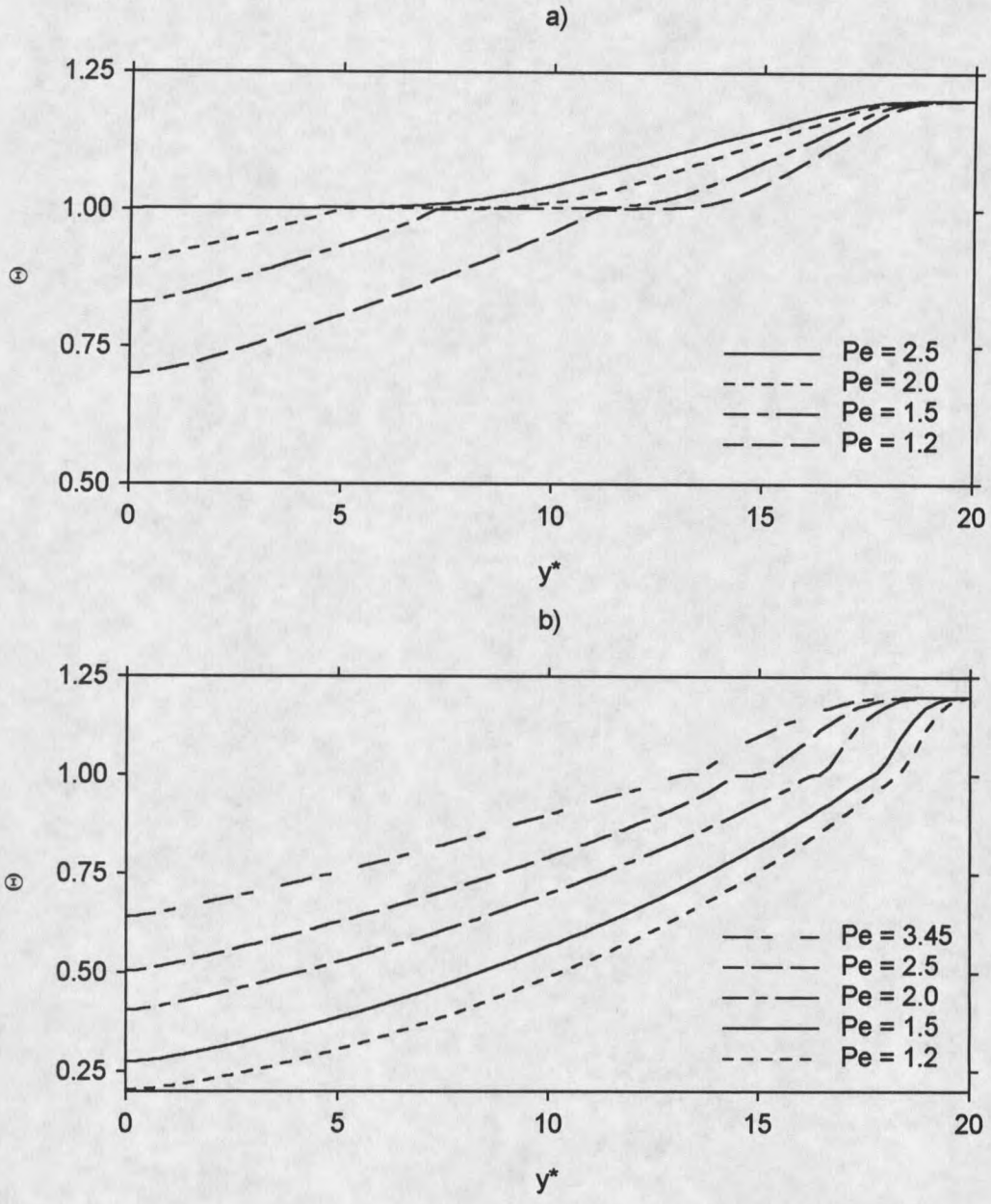

Figure 14. Centerline temperature for (a) $Bi_2 = 0.0249$, $Bi_3 = 0.042$; (b) $Bi_2 = 0.0748$, $Bi_3 = 0.1261$.

Figure 15 shows the local heat flux as a function of length along the outer edge of the cast metal for different *Pe*. The plot is for the following casting conditions; Θ_0 = 1.2, Bi_2 = 0.0748, Bi_3=0.1261, Pe = 1.2, 1.5, 2.0, 2.5, 3.45. Increasing withdrawal speeds resulted in higher heat fluxes throughout the entire domain. Higher withdrawal speeds resulted in more heat being convected further downstream. Therefore the local heat flux value increased everywhere along the outer edge. At the mold exit there was a discontinuity in the Biot number ($Bi_2 \neq Bi_3$). A discontinuous cooling rate at that point disrupted the smooth heat flux function on both sides of the mold exit, as illustrated in Figure 15.

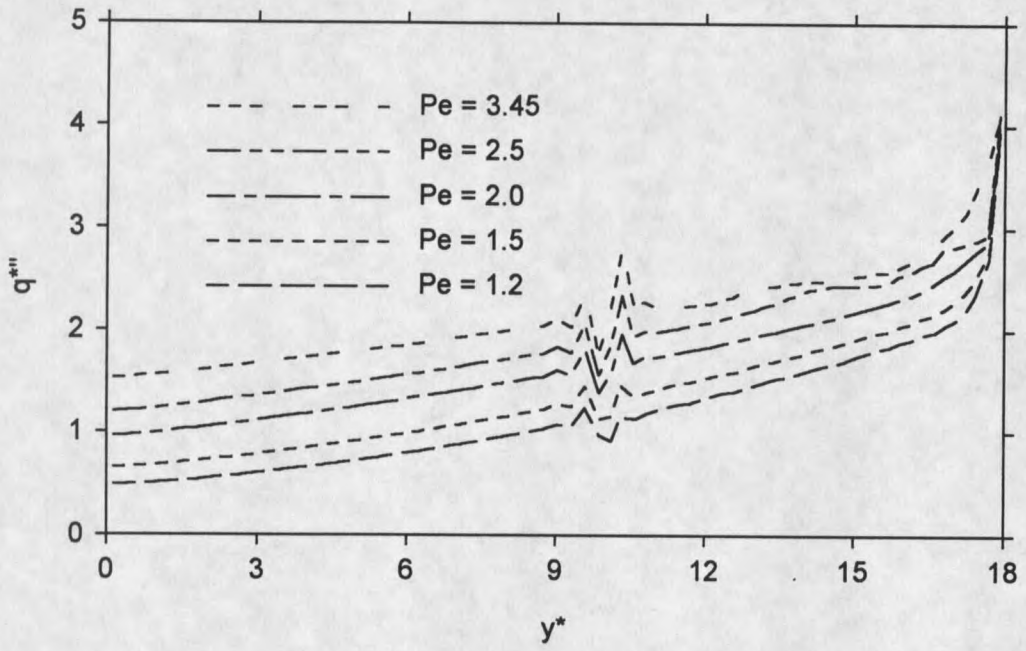

Figure 15. Withdrawal speed effect on local heat flux. Θ_0 = 1.2, Bi_2=0.0748, Bi_3 = 0.1261, Pe = 1.2, 1.5, 2.0, 2.5, 3.45.

Numerical results indicate that most of the heat is extracted in the mold region. That is due to the fact that a large amount of latent heat has to be extracted in this region, for the change of phase to occur inside the mold and to prevent breakup.

Various conditions were simulated to investigate the heat flow rate out of the cast metal. In this section, only the effect of the Peclet number on the total amount of heat extracted from the metal is considered. The amount of heat extracted in the mold as a fraction of the total heat flux is plotted with increasing Peclet number in Figure 16. The figure shows that with increasing withdrawal velocity, the portion of the heat removed by the mold decreases slightly. However, it stays around 78 – 80% for a range of Pe = 1.0 – 2.5.

With the increasing Peclet number the total heat flux was expected to increase for the following reasons. Figures 11 and 12 illustrated that with increasing Peclet number the solidification front moved downstream, which increased the temperature throughout the cast material and the mold. Increased outer boundary temperatures throughout the domain resulted in a higher temperature difference between the outside of the mold (and the outside edge in the post-mold region) and the surrounding air. Under assumption of constant convective heat transfer coefficients, a larger temperature difference reflects directly in higher heat flux values.

In Figure 17, the average dimensionless heat flux is plotted as a function of the Peclet number (Pe = 1 - 2.5). It was observed that the heat flux increases

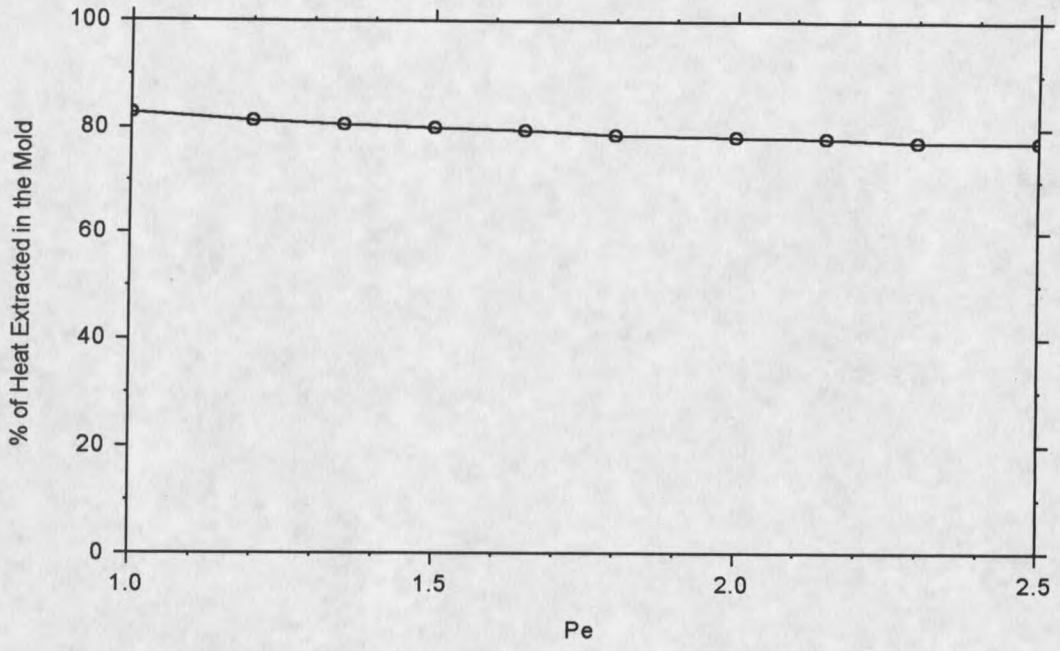

Figure 16. Percentage of total heat flux extracted in the mold. Pe effect.

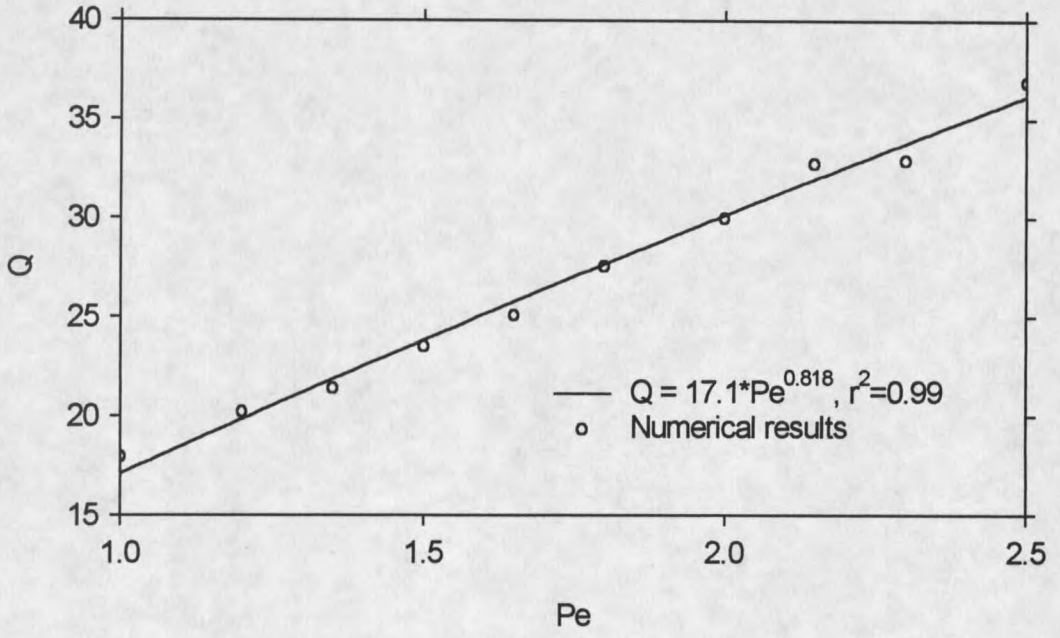

Figure 17. Average heat flux as a function of the Peclet number.

$\Theta_0 = 1.2$, $Bi_2 = 0.0748$, $Bi_3 = 0.1261$.

with the increasing Peclet number regardless of the cooling rate in the mold and post-mold regions. This is because the higher withdrawal velocities cause more superheat to be convected further downstream into the mold and post mold regions, where the heat is extracted. Whereas Kang and Jaluria (1993) investigated the lower Peclet number range (0.3 to 1.0), the present work included a wider range of Peclet numbers (1.0 to 3.45). The range of Peclet numbers extended up to the point when cases became numerically unstable. The amount of superheat and the cooling rates were held constant at Θ_0 = 1.2, Bi_2 = 0.0748, Bi_3 = 0.1261. A correlation between the Peclet number and the dimensionless heat flux, Q, was obtained by curve-fitting the numerical results. The derived expression for given conditions is:

$$Q = 17.1 \cdot Pe^{0.818} \tag{4.8}$$

Statistical significance of the above correlation was checked by calculating the r^2 parameter. r^2 is defined as the variance in the fitted model divided by the variance in the numerically obtained data. r^2 can be written as:

$$r^2 = \frac{\sum (Q_j^0 - Q_{av})^2}{\sum (Q_j - Q_{av})^2} \tag{4.9}$$

In equation (4.9) superscript '0' denotes the fitted data (Eq. 4.8), Q_j represents the numerically obtained total heat flux (Eq. 4.7), and Q_{av} denotes the

average of numerically obtained results. It was found that r^2 = 0.99. The maximum deviation was found to be 0.856, which is 3% of the average heat flux (Q_{av}=26.91) obtained by integration. Therefore, the data fit in equation (4.8) was considered statistically significant for the given casting conditions.

As discussed earlier, for the second set of input parameters plotted in Figure 11(b) (Θ_0 = 1.2; Bi_2 = 0.0748; Bi_3 = 0.1261; Pe = 1.2, 1.5, 2.0, 2.5, 3.45), it was not possible to reach the breakout conditions. In attempting to move the solidification front beyond the mold, the Peclet number was increased over 3.45. This resulted in numerical instability. To demonstrate the breakout conditions with the increasing *Pe*, the cooling rates had to be lowered (Bi_2 = 0.0249, Bi_3 = 0.042).

It was observed that the cooling rate has similar effects on the numerical stability of the test cases. Higher heat removal cases were easier to control than the lower cooling rate cases. The effect of the cooling rates on the solidification process is discussed later in a separate section.

Effects of Superheat

As discussed earlier, in this research superheat is defined as the difference between the solidification temperature and the temperature at the inlet. The superheat temperature had the most direct influence on the solidification process. It affected the solidification front position and the heat flux directly. The effects of changing the values of superheat were studied by obtaining the numerical results for the following two sets of input parameters:

- Pe = 1.5, 2.0; Bi_2 = 0.0748; Bi_3 = 0.1261; Θ_0 = 1.2, 1.5, 2.0, 2.5, 2.7
- Pe = 2.5, 2.0; Bi_2 = 0.0748; Bi_3 = 0.1261; Θ_0 = 1.2, 1.5, 2.0

As expected, the amount of superheat has a strong influence on the temperature distribution within the cast material. For both sets of input parameters it was possible to reach the breakout conditions. The amount of superheat greatly affects the position of the solidification front. This indicates that lower casting speeds should be used for large amounts of superheat. Solidification front positions for the above two sets of inputs are shown in Figure 18.

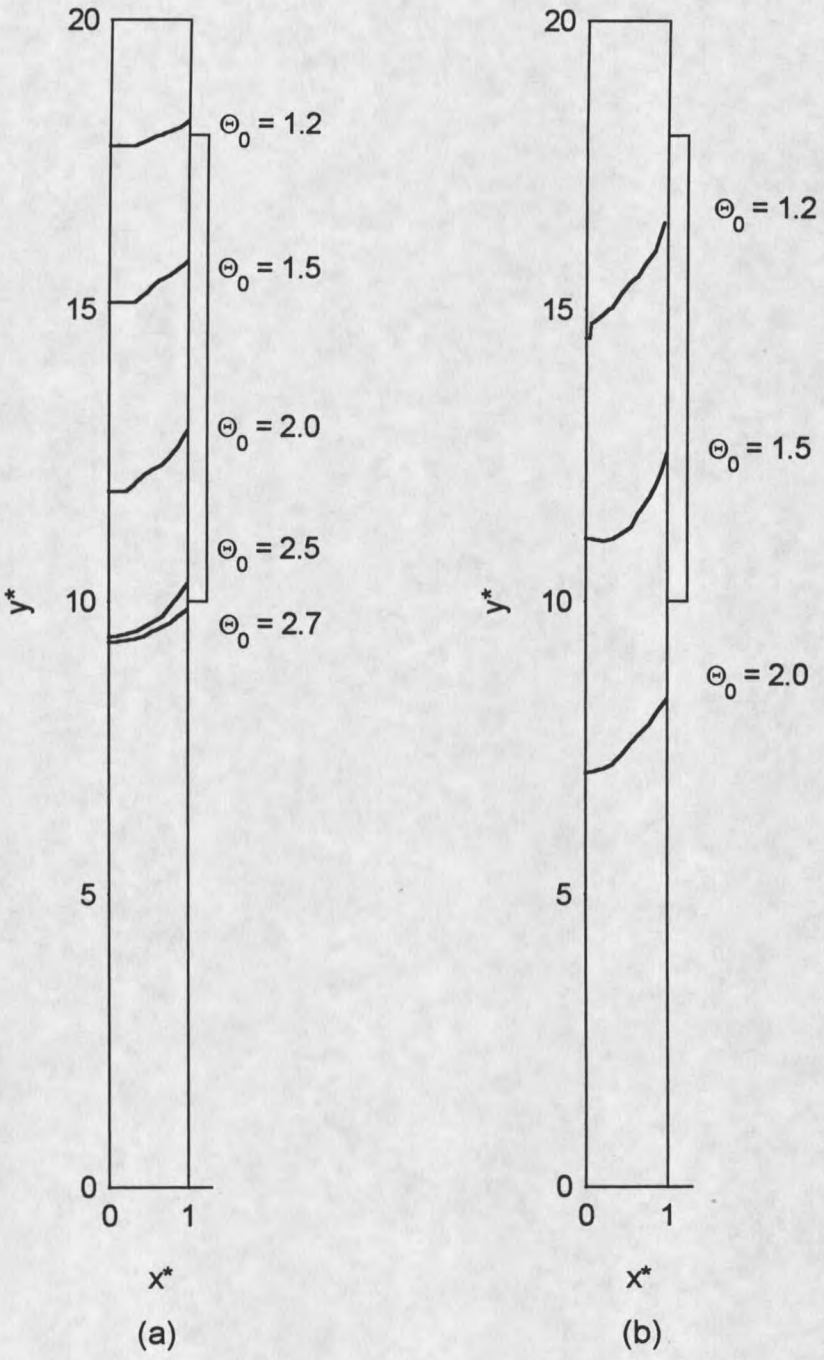

Figure 18. Superheat effect on solidification front position. (a) Pe = 1.5; Bi_2 = 0.0748; Bi_3 = 0.1261; (b) Pe = 2.5; Bi_2 = 0.0748; Bi_3 =0.1261.

From Figure 18, it can be noted that superheat amount does not affect the solidification front slope significantly. For the lower Peclet number cases the slope is flatter, which is desired in order to get better uniformity in the cast product, as reported by Kang and Jaluria (1993). Therefore, the amount of superheat is not a suitable parameter to control the slope of the solidification interface.

Figure 19 shows the local dimensionless heat flux as a function of length along the outer surface of the casting. The plot is for the following casting conditions; Pe = 2.5, Bi_2 = 0.0748, Bi_3 = 0.1261, Θ_0 = 1.2, 1.5, 2.0. The plots suggest that higher amounts of superheat result in higher local heat flux values. The reason is that in case of higher superheat, more total heat needs to be extracted for solidification to occur. Higher initial temperature results in higher temperatures along the outer edge, and therefore in higher temperature difference between the surface and ambient temperatures. The consequence is higher local heat flux throughout the investigated domain.

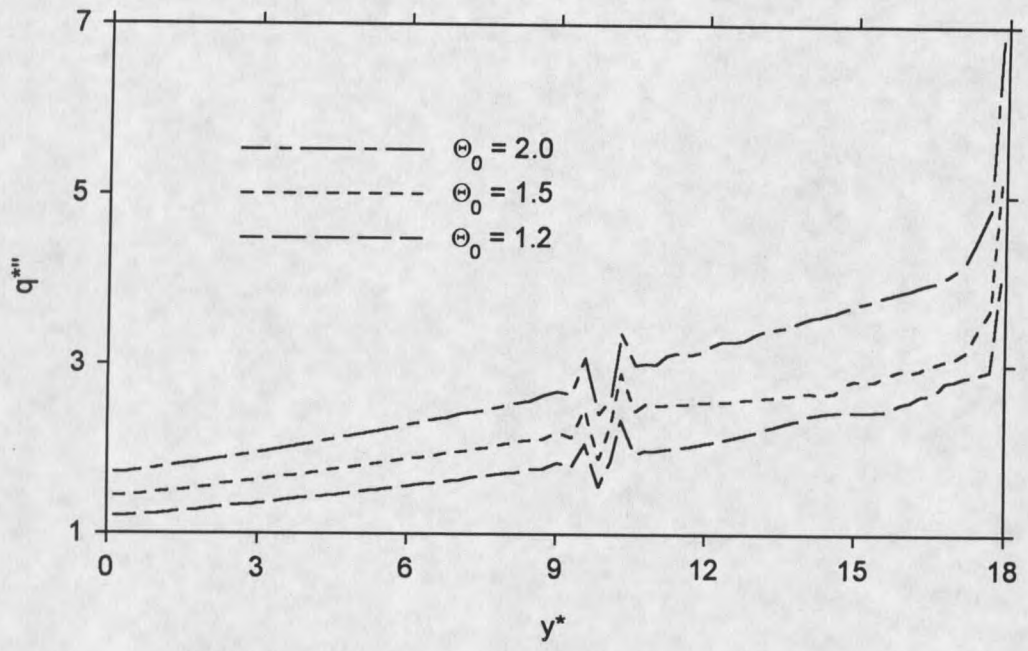

Figure 19. Superheat effect on local heat flux. Pe = 2.5, Bi_2 = 0.0748, Bi_3 = 0.1261, Θ_0 = 1.2, 1.5, 2.0.

Temperature distribution along the outer surface has a direct effect on the total heat flux. Figure 20 and Figure 21 show the temperature profiles along the outer surface and along the centerline of the cast material as a function of superheat, Θ_0. Due to no heat transfer in the pre-mold region (y* = 18 - 20), the temperature gradient at the entrance of the computational domain is zero. Near the mold entrance (y*~18) the temperature starts to decrease, which is due to the conductive heat transfer in the axial direction. This effect shows that axial diffusion of thermal energy is important and should be considered.

Similarly to the study of the Peclet number effect, higher temperature along the outside of the casting suggests that the heat flux should increase with the higher amount of superheat. This happens because with increased inlet temperature, a larger amount of heat must be removed in the mold and post-mold regions. Figure 22 shows the total dimensionless heat flux out of the material as a function of the superheat. A strong influence of the amount of superheat on the heat flux was observed.

A correlation between the total heat flux, Q, and the superheat, Θ_0, was obtained for the cases with Pe = 1.5, Bi_2 = 0.0748, Bi_3 = 0.1261, and Θ_0 = 1.2 - 2.7, (Figure 22). The correlation is expressed by equation (4.10).

$$Q = 18.1 \cdot \Theta_0^{1.71} \qquad (4.10)$$

Statistical check was carried out to verify the validity of equation (4.10). It was calculated that r^2 = 0.999. The maximum deviation was 1.77, which is 2.9% of the average heat flux obtained by integration (Q_{av}=60.84). r^2 is very close to unity, which is required. Therefore, the relation was considered significant for given casting conditions.

Figure 23 shows the percent of the total heat removed by the mold region. The fraction of total heat removed by the mold remains nearly unaffected with

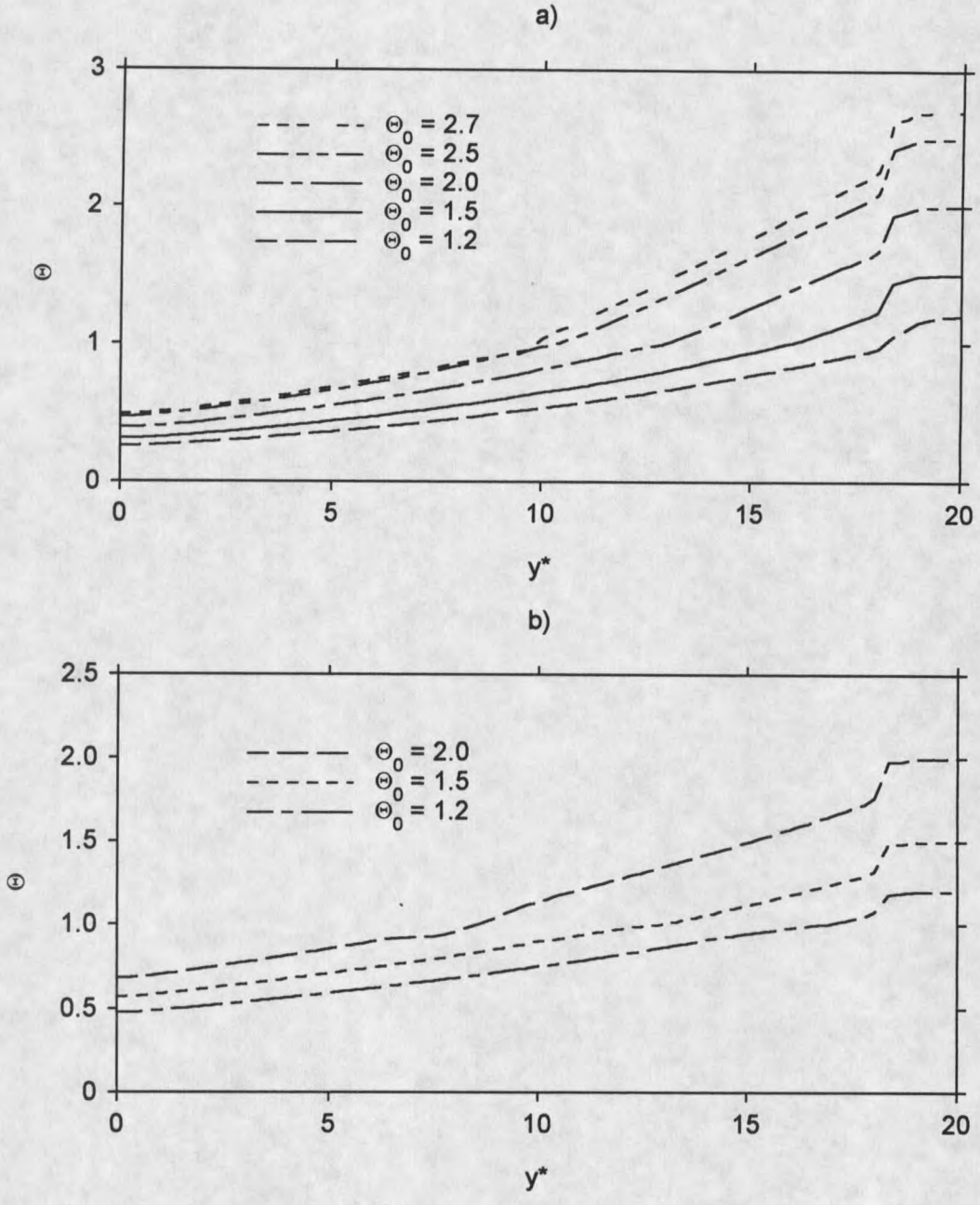

Figure 20. Outer surface temperature for $Bi_2 = 0.0748$, $Bi_3 = 0.1261$;

(a) Pe = 1.5, (b) Pe = 2.5.

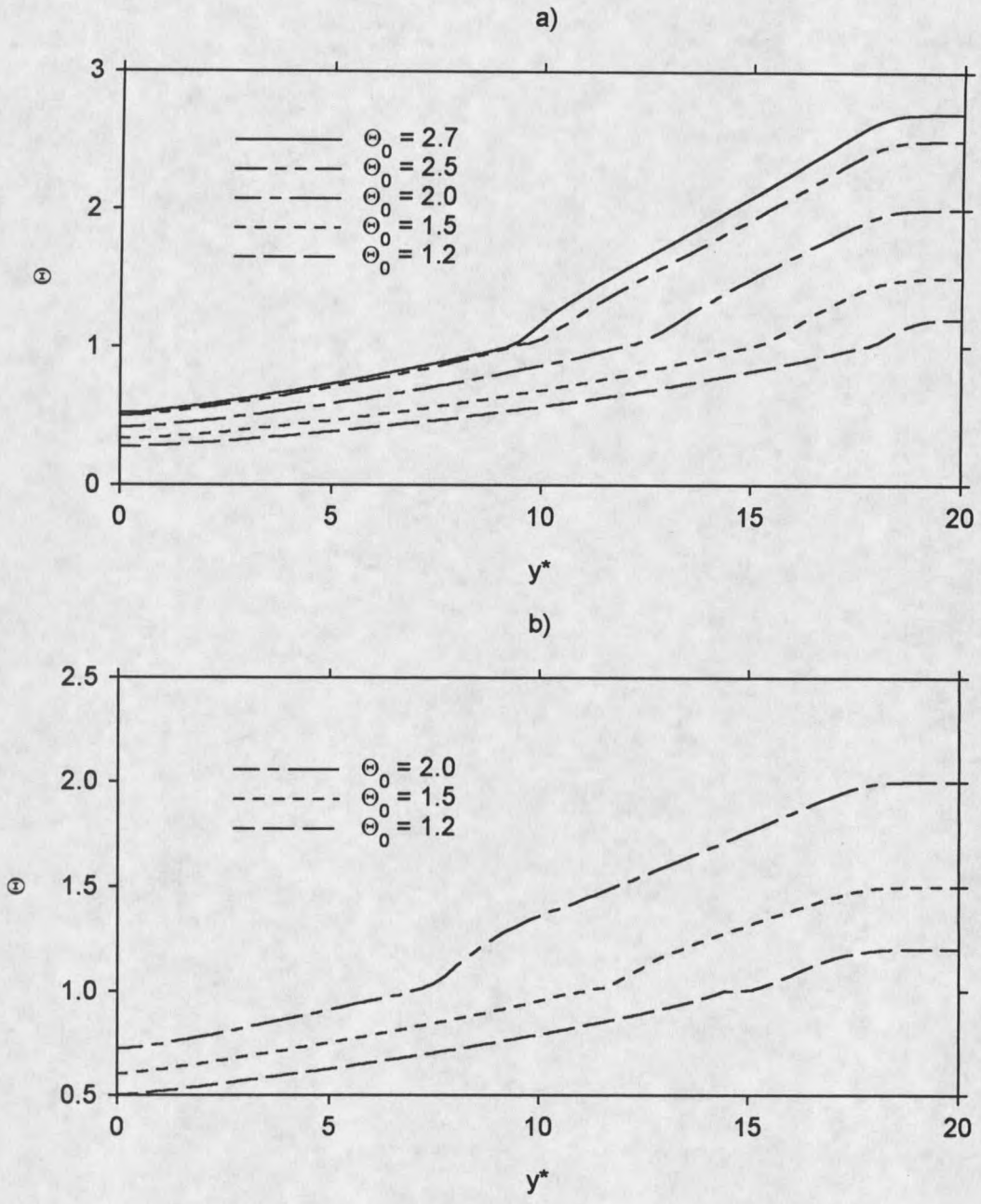

Figure 21. Centerline temperature for $Bi_2 = 0.0748$, $Bi_3 = 0.1261$;

(a) Pe = 1.5, (b) Pe = 2.5.

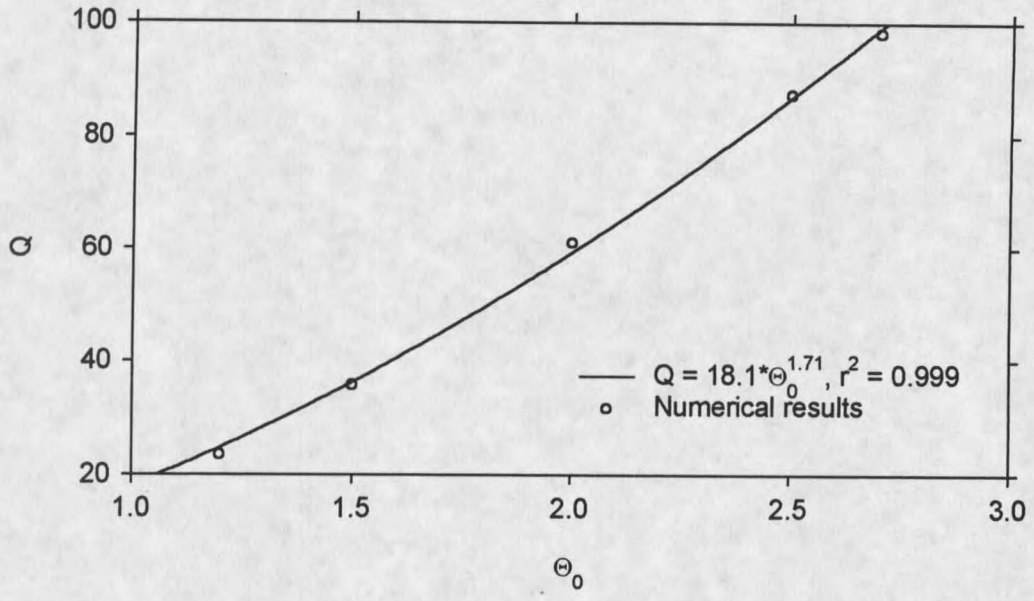

Figure 22. Total heat flux as a function of Θ_0. $Bi_2 = 0.0748$, $Bi_3 = 0.1261$, Pe = 1.5, Θ_0 = 1.2, 1.5, 2.0, 2.5, 2.7.

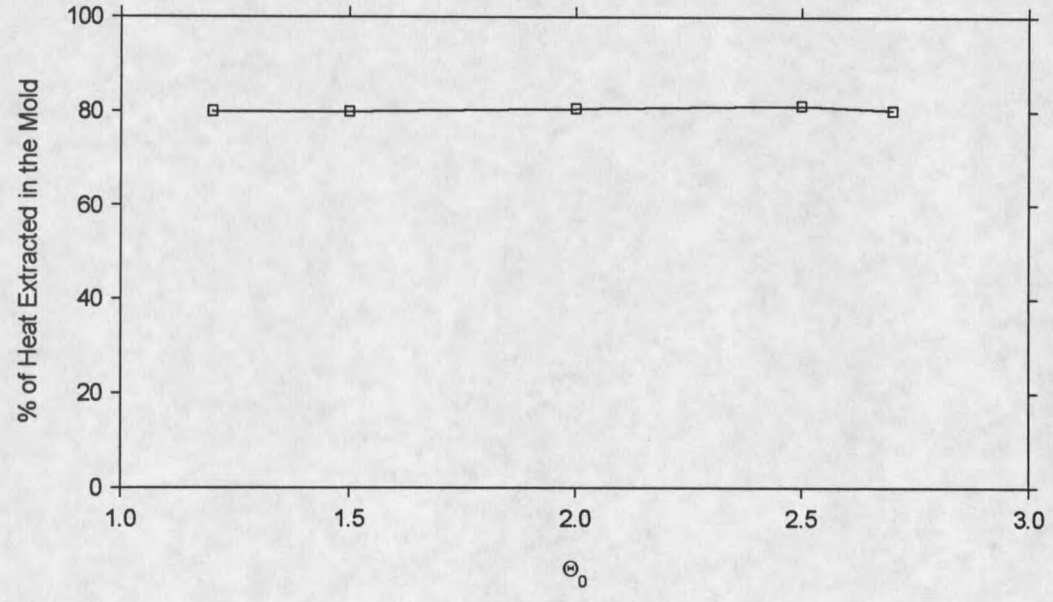

Figure 23. Percentage of total heat extracted in the mold - Θ_0 effect.

increasing superheat. The same observations were made by Huang et al. (1992) in studying the superheat removal from the continuously cast steel slabs.

Effects of Radiation

As described earlier, radiation between the cast material and the mold was investigated. In the process of cooling below the solidus temperature, the material shrinks and an interfacial air gap is formed. It was found by Ho et al. (1985) that the overall interfacial heat transfer coefficient is decreased due to limited contact. It was discussed by the same author that the overall heat transfer coefficient along the inside of the mold decreases by as much as 50%. The study concluded that changing interfacial thermal conductance has an effect on the solidification time and the nature of solidification.

For the reasons mentioned above, it was expected that the radiation would have a noticeable effect on the heat transfer rate through the mold. The solidification front position was expected to change due to a higher heat removal rate.

However, these predictions proved to be inaccurate. Several cases were run varying the inlet parameters and cooling conditions. It is important to note at this point that the radiation boundary condition only applies in the solid portion of the flow, i.e. beyond of point of freezing. The solidification front location was not affected when applying the radiation boundary condition beyond the point of

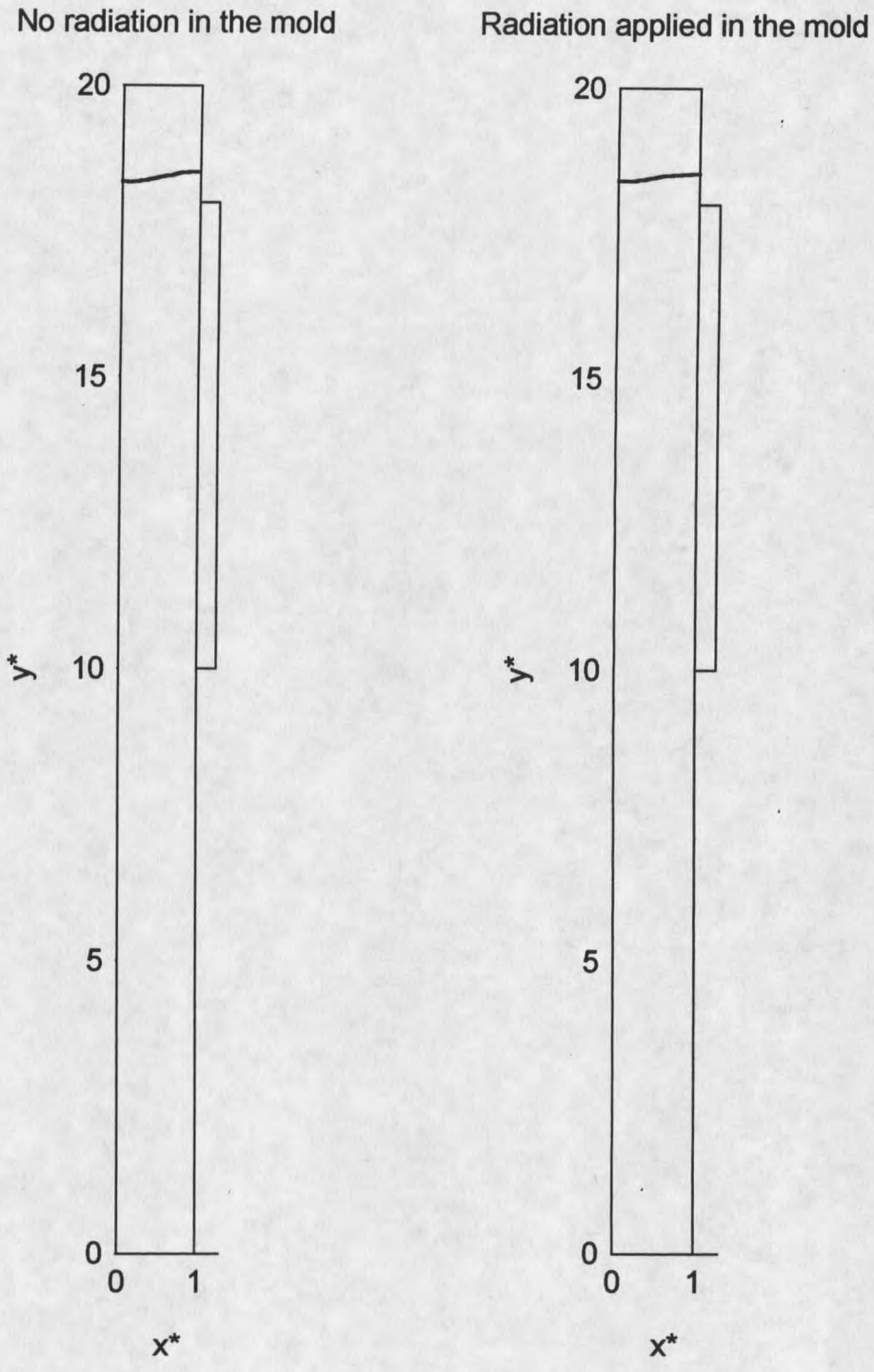

Figure 24. Effect of radiation in the mold region on solidification front position; Pe = 1.2, Θ_0 = 1.2, Bi_2 = 0.0748, Bi_3 = 0.1261.

freezing. Especially in cases with lower casting velocities, when solidification occurs early in the mold region, the radiation was expected to have an effect.

The driving force for the radiative heat flux is the temperature difference between the two surfaces. In our case the shape factor was assumed equal to unity. The solidification front locations are presented in Figure 24, which shows essentially no difference in the location of the solidification front, when the radiation was applied. This is consistent with the temperature difference between the solidified metal and the inside surface of the mold material, as shown in Figure 25. The temperature profiles in Figure 25 show that the temperature difference between the cast metal and the inside surface of the mold is not sufficient to result in a large enough radiative heat flux.

Next, two cases were investigated to explore whether a larger amount of superheat would result in a larger temperature gradient along the inside of the mold. The input parameters were chosen so that solidification still occurred far enough upstream for radiation to take place.

Figure 26 shows the temperature along the mold/metal interface ($x^* = 1$, $y^* = 10$ -18) for two different amounts of superheat. The difference in temperature for all cases is extremely small. In Figure 26 it is virtually impossible to distinguish between the two temperatures. This is the reason for a negligible effect of the radiation mechanism on the temperature distribution and therefore on the total heat flux.

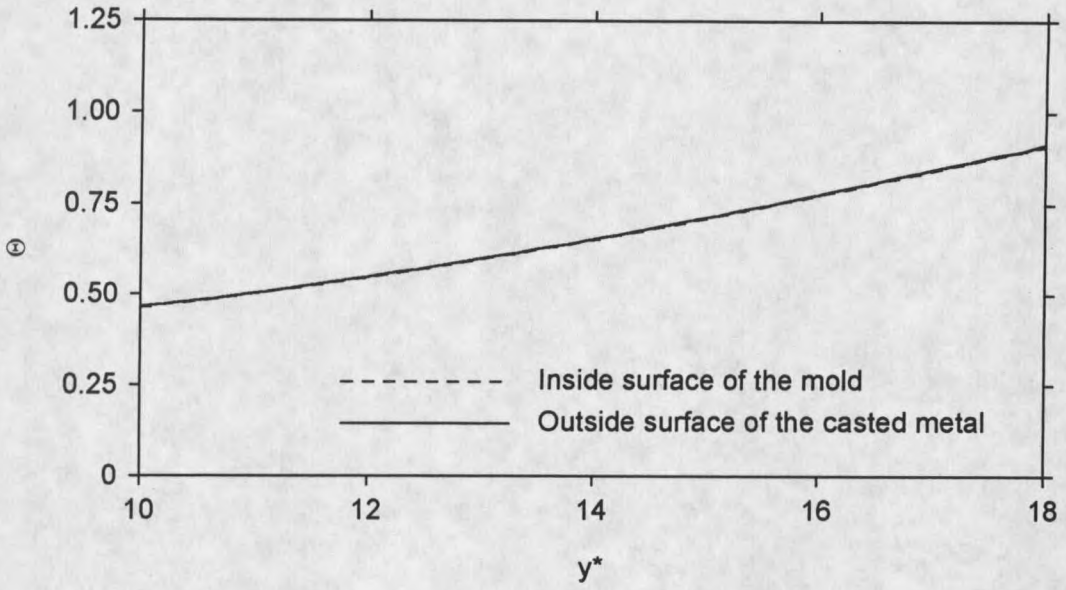

Figure 25. Temperature distribution in the mold region; Pe = 1.5,

Θ_0 = 1.2, Bi_2 = 0.0748, Bi_3 = 0.1261.

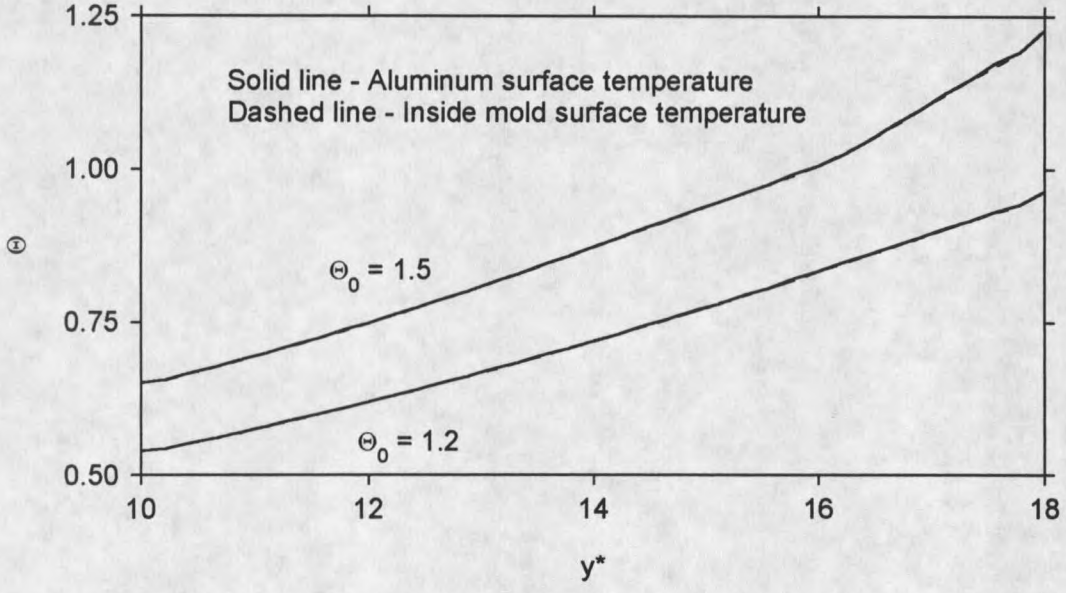

Figure 26. Effect of superheat on radiation in the mold region;

Pe = 1.5, Bi_2 = 0.0748, Bi_3 = 0.1261, Θ_0 = 1.2, 1.5.

Effect of Cooling Rate

Cooling rates in the mold and post-mold regions had a direct and a very significant effect on the solidification process. The rate of cooling affected the physical behavior of the material under consideration. Solidification front position, total heat flux, and the temperature profiles throughout the casting were greatly affected. In this research the pre-mold region ($y^* = 18 - 20$) was assumed to be insulated. Constant values of convective heat transfer coefficient were assigned in the mold and post-mold regions. The non-dimensional mold and post-mold convective heat transfer coefficients were expressed as Bi_2 and Bi_3 respectively.

Mold Cooling Rate Significance

Besides the amount of superheat, the convective heat transfer coefficient in the mold region was found to have the strongest effect on the solidification process. Several cases were run to investigate the importance of the mold cooling rate, Bi_2. The amount of superheat was taken as constant at Θ_0=1.2. Two different casting speeds were investigated; Pe = 1.2, 1.5. The mold cooling rates were taken as Bi_2 = 0.0249, 0.0499, 0.0748. In dimensional terms, these Biot numbers represent the heat transfer coefficient of h_2 = 1000, 2000, 3000 W/m^{2}K respectively.

The two most important parameters affecting the quality of the cast product are the mold cooling rate, Bi_2, and the withdrawal speed, Pe.

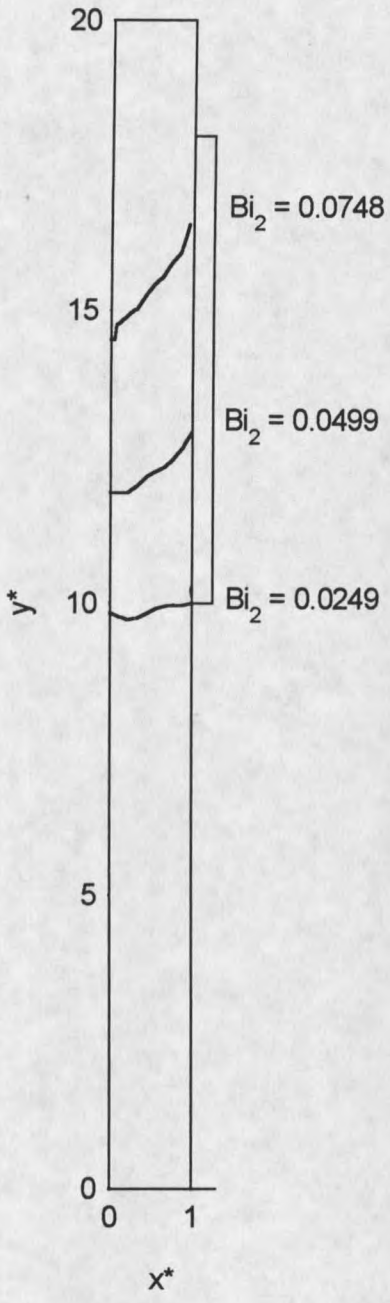

Figure 27. Effects of mold cooling rate on solidification front position;

Pe = 2.5, Θ_0 = 1.2, Bi_3 = 0.1261, Bi_2 = 0.0748, 0.0499, 0.0249.

First let us consider the effects of Bi_2 on the physics of the solidification process. Figure 27 illustrates its effect on the solidification front position. The post mold Biot number was fixed at $Bi_3 = 0.1261$.

From Figure 27 we can see that the convective cooling rate on the outside of the mold, Bi_2, strongly affects the solidification front position. Increasing the value of Bi_2 not only affects the location of the freezing front, but also strongly influences its slope. The slope of the front is important in achieving the uniformity in the cast product, Kang and Jaluria (1993). The microstructure of the cast product is dendritic, more dense and uniform when the material undergoes the same treatment throughout the mold. The material becomes less dense and uniform when the interface slope becomes steep.

The other parameter controlling the interface slope is the withdrawal speed. Lower withdrawal speeds decrease productivity and higher cooling rates increase the production cost. Therefore, a cost-effective combination between these two parameters is desired.

Figure 27 demonstrates that it is possible to reach breakup conditions for the lowest mold Biot number, $Bi_2 = 0.0249$. This indicates that for given casting conditions, a minimum safe mold cooling rate exists. For lower value of Bi_2, breakout will occur because the solidification front will move beyond the mold region.

Figure 28 shows the local dimensionless heat flux, as a function of length along the outer surface of the casting. The plot is for the following casting

conditions; Pe = 1.2, Θ_0 = 1.2, Bi_3 = 0.1261, Bi_2 = 0.0249, 0.0499, 0.0748. The figure shows that higher mold cooling rates result in higher local heat flux value. There is a disruption in local heat flux values at the mold exit (y* = 10), due to a sudden change in cooling rates.

It was observed that lower mold cooling rates (Bi_2 = 0.0249) result in higher post-mold heat flux values. When Bi_2 is low and low amounts of heat are extracted from the mold, the cast material beyond the mold still carries a relatively high amount of energy. The temperature of the casting at the mold exit is higher due to smaller values of Bi_2, as illustrated in isotherm plots later in this chapter. Since higher surface temperatures occur for the casting, a larger temperature difference will be exhibited between the casting surface and the ambient air. As a result, the local heat flux increases in the post-mold region.

The opposite effect is observed when the mold cooling rate is high (Bi_2 = 0.0748). In this case, the heat flux values in the mold region are high, resulting in lower surface temperatures of the casting at the mold exit and therefore lower heat flux values result in the post-mold region.

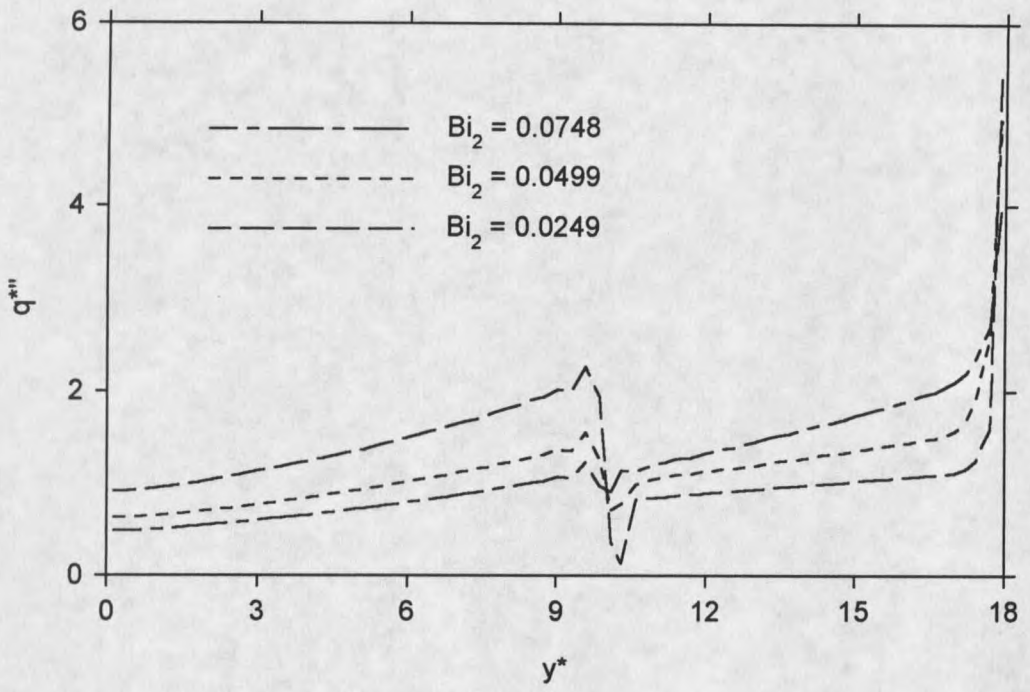

Figure 28. Mold cooling rate effect on local heat flux. Pe = 1.2, Θ_0 = 1.2, Bi_3 = 0.1261, Bi_2 = 0.0249, 0.0499, 0.0748.

The influence of the mold Biot number, Bi_2, on the total heat flux was then investigated. Since temperature fields are strongly dependent on the cooling rates, Bi_2 was expected to have a strong influence on the total heat flux. Two casting speeds were investigated; Pe = 1.2, 1.5. Superheat was fixed at Θ_0 = 1.2. Figures 29 illustrates the total heat flux as a function of Bi_2.

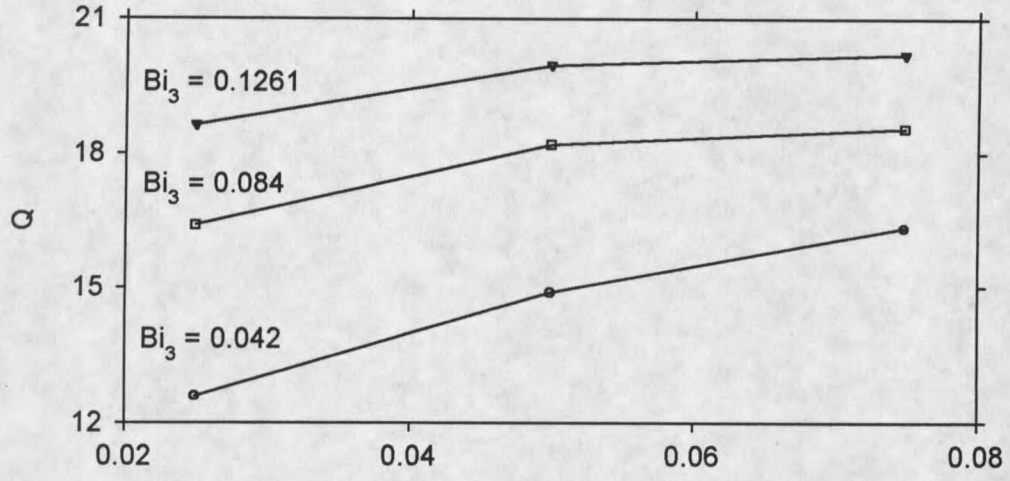

(a) Pe = 1.2, Θ_0 = 1.2

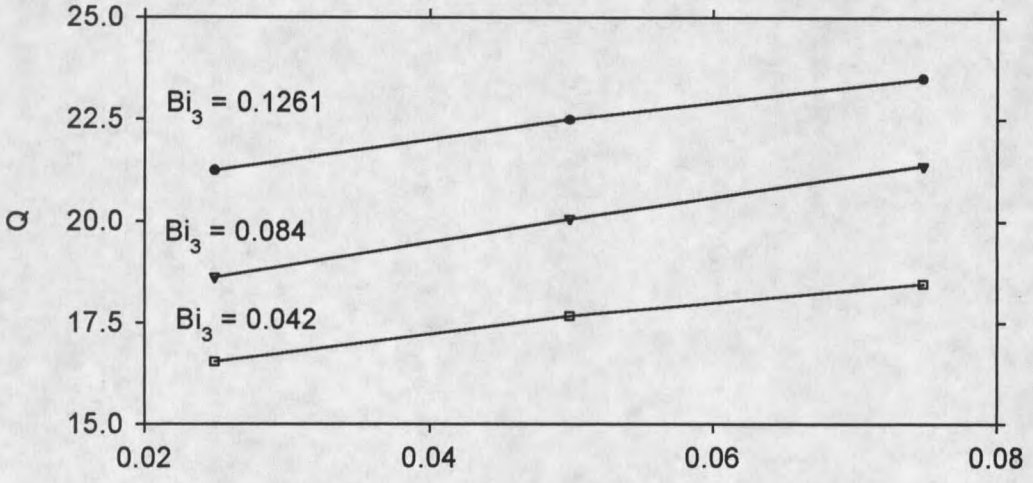

(b) Pe = 1.5, Θ_0 = 1.2

Figure 29. Mold cooling rate effect on the total heat flux.

As expected, the mold cooling rates had a direct effect on the total heat flux, regardless of the casting parameters (Figure 29).

A more interesting comparison arises when the percentage of the total heat transfer extracted by the mold is observed. The percentage of the total heat removed in the mold region vs. Bi_2 is plotted in Figure 30. The figure shows that most of the total heat was removed in the mold. Huang et al. (1990) studied this effect and found that the percentage of heat extracted by the mold stays about constant at approximately 60%.

In the present study it was found that the percentage of heat removed through the mold is directly proportional to the heat transfer coefficient for that region. Heat removal percentages were found to be higher than the results presented by Huang et al. (1990). In their study the inlet temperature of steel equaled 1813K and the solidification temperature was 1783K, resulting in a relatively low amount of superheat (Θ_0 = 1.02). The inlet temperature suggested that a higher amount of total energy had to be removed than in the present study, where the inlet temperature was 1117K and the solidification temperature was 933.52K (Θ_0 = 1.2).

The percentage of the total heat increased with increasing Bi_2 (Figure 30), and heat removal became a concern. As the withdrawal speed increased, the heat flux increased as discussed earlier. The maximum heat removal rate for a specific mold will eventually be reached.

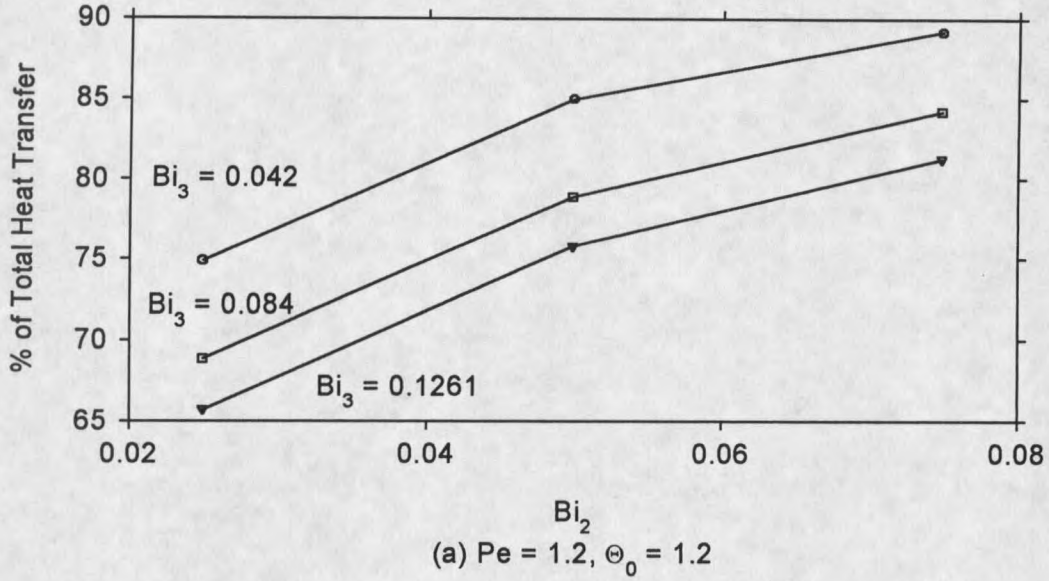

(a) Pe = 1.2, Θ_0 = 1.2

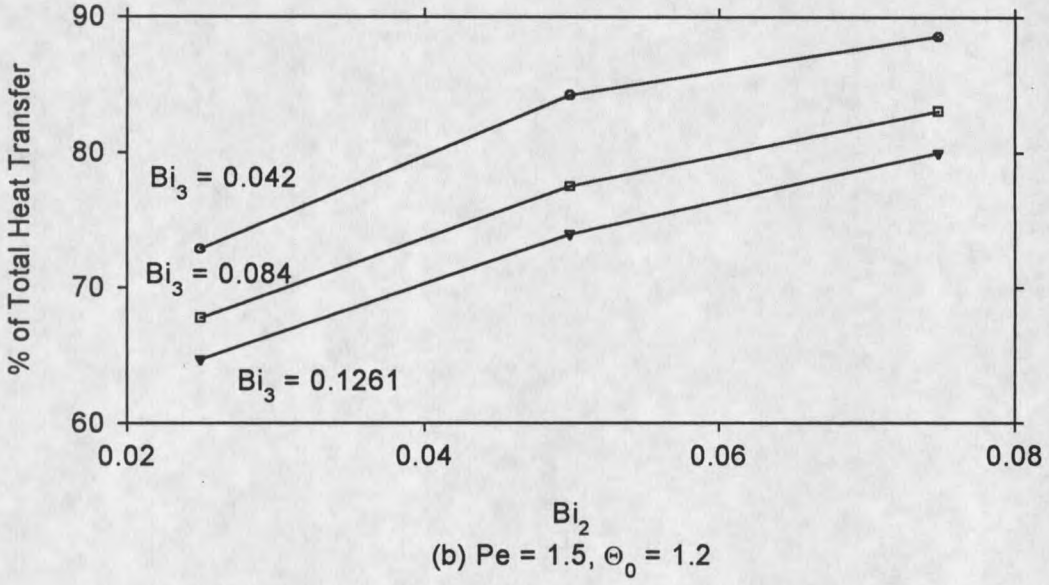

(b) Pe = 1.5, Θ_0 = 1.2

Figure 30. Percentage of total heat removed by the mold. Bi_2 effect.

Cases for different post-mold cooling rates (Bi_3 = 0.042, 0.084, 0.1261) showed similar trends. For both casting speeds (Pe = 1.2, 1.5), Figure 30 shows a stronger effect on the total portion of heat removed in the mold when Bi_2 is increased from 0.0249 to 0.0499, than during the increase from 0.0499 to 0.0748. This observation suggests that there is a maximum amount of heat that can be removed by the mold. This finding was related to the physical limitation on a specific mold, which depends on the type of the mold (shallow water-circulated or solid metal), mold material, and intensity of forced convection applied to mold and post-mold surfaces.

The relation between the surface heat transfer coefficient and the surface temperature offers another comparison. Temperature distributions along the outside surface of the cast material were plotted in Figure 31 for cases with Pe = 1.2, Θ_0 = 1.2. It was previously proven that the cooling rate in the mold region greatly affects the heat flux (Figure 29). Therefore, the temperature profile was also drastically affected by the value of Bi_2.

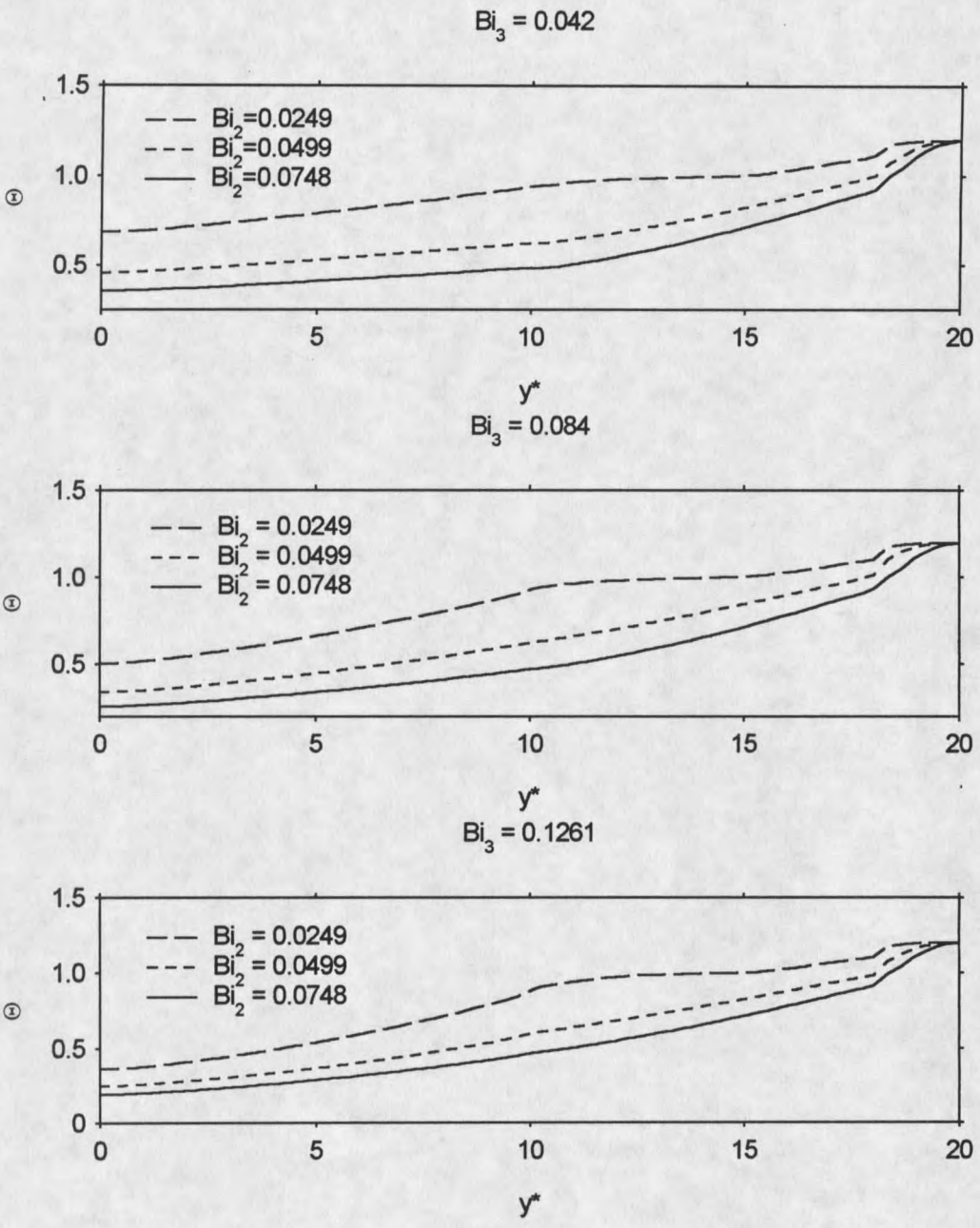

Figure 31. Effects of mold cooling rate on the outside surface temperature; Pe=1.2, Θ_0 =1.2; Bi_2 = 0.0249, 0.0499, 0.0748; Bi_3 = 0.042, 0.084, 0.1261

Post-Mold Cooling Rate Significance

Post-mold cooling rate was found to be a significant factor in the continuous casting process as well. The mode of heat transfer in the post-mold region was assumed to be forced convection. Free convection forces were not neglected, but were found to have negligible effect on the solidification mechanism. According to Huang et al. (1992) the inertial forces are at least five times more important than the buoyancy forces. Choudhary and Mazumdar (1995) also reported that thermal natural convection phenomena plays an insignificant role in continuous casting.

Numerical cases included the following conditions. The amount of superheat was taken as constant at $\Theta_0 = 1.2$. Two different casting speeds were investigated; Pe = 1.2, 1.5. The non-dimensional post-mold cooling rates were taken as $Bi_3 = 0.042, 0.084, 0.126$. In dimensional from these Biot numbers represent the heat transfer coefficient of $h_3 = 1000, 2000, 3000$ W/m^{2}K respectively. Although these dimensional convective heat transfer coefficients have the same values as described for the mold region, the respective non-dimensional parameters are not the same. That is due to the definition of the Biot number, which includes the thermal conductivity. In the post-mold region, the material undergoing the forced convection is solid aluminum, whereas in the mold region it is the mold (solid copper) that is exposed to convective forces.

Unlike the effects of the mold cooling rate, the post-mold cooling rate was found to have a negligible effect on the solidification front position ($\Theta = 1$).

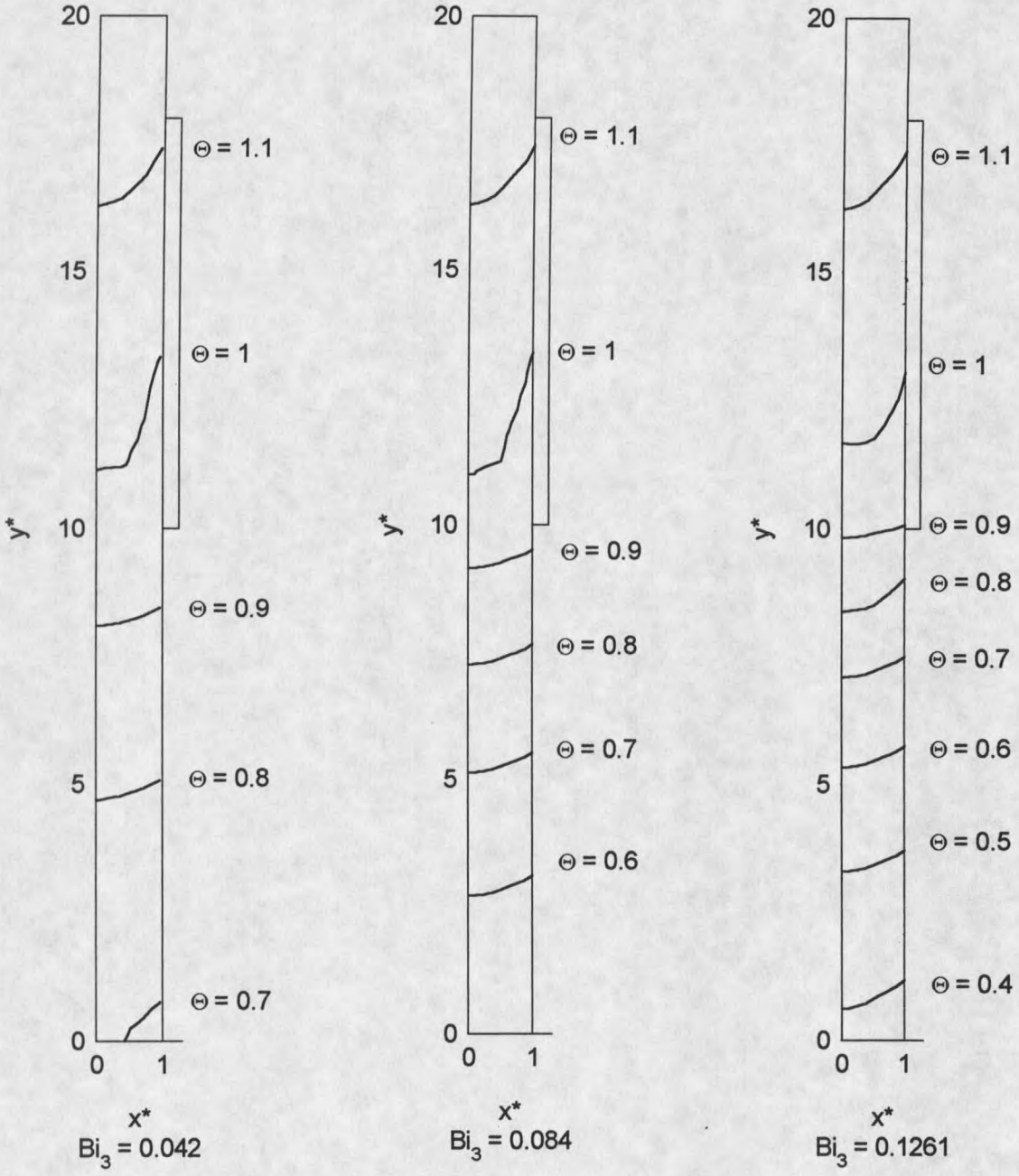

Figure 32. Effect of post-mold cooling rate on temperature distribution;

Pe=1.2, Θ_0=1.2,Bi_2 =0.0249, Bi_3=0.042, 0.084, 0.1261.

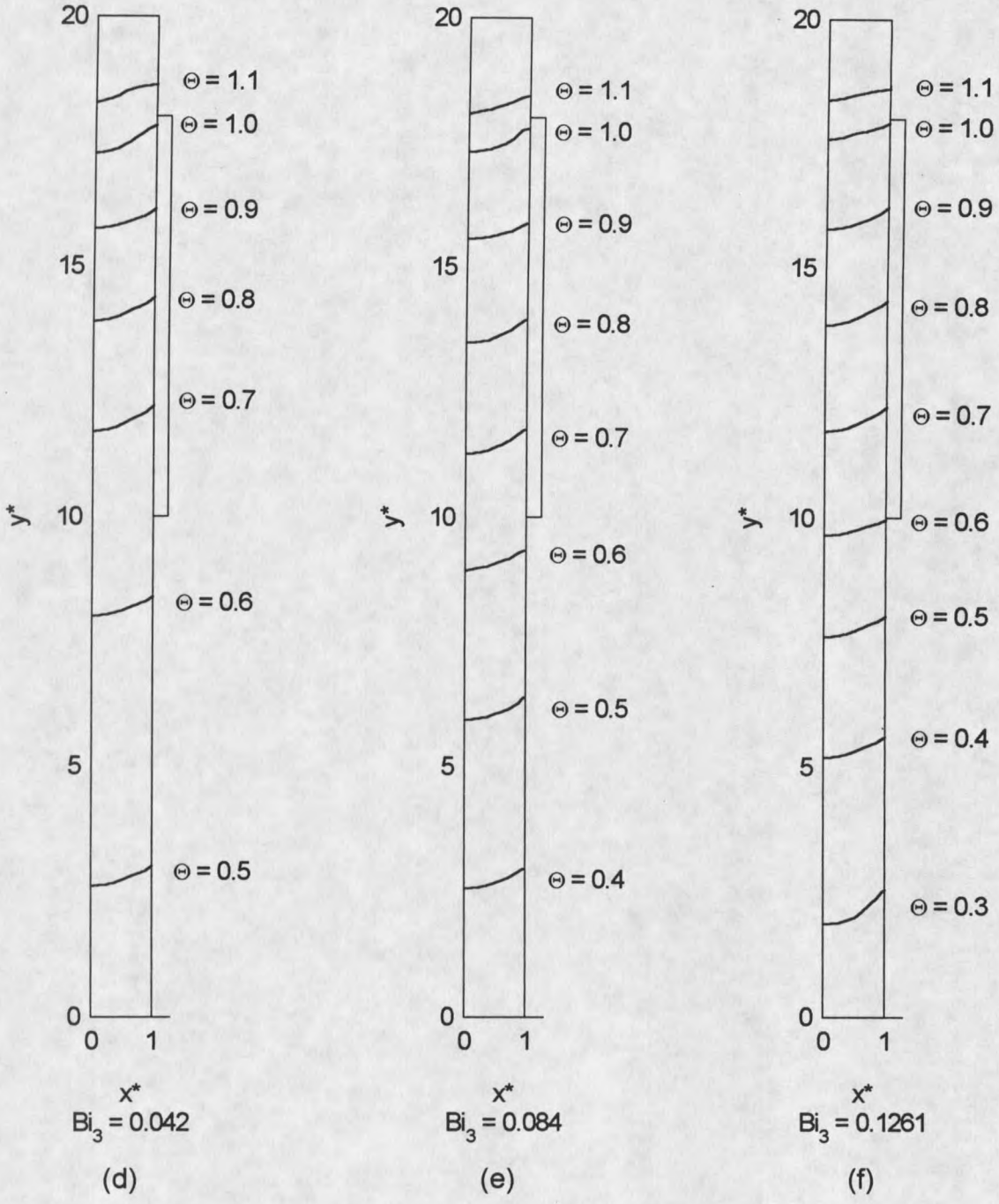

Figure 32 cont. Pe=1.2, Θ_0=1.2, Bi_2 = 0.0499

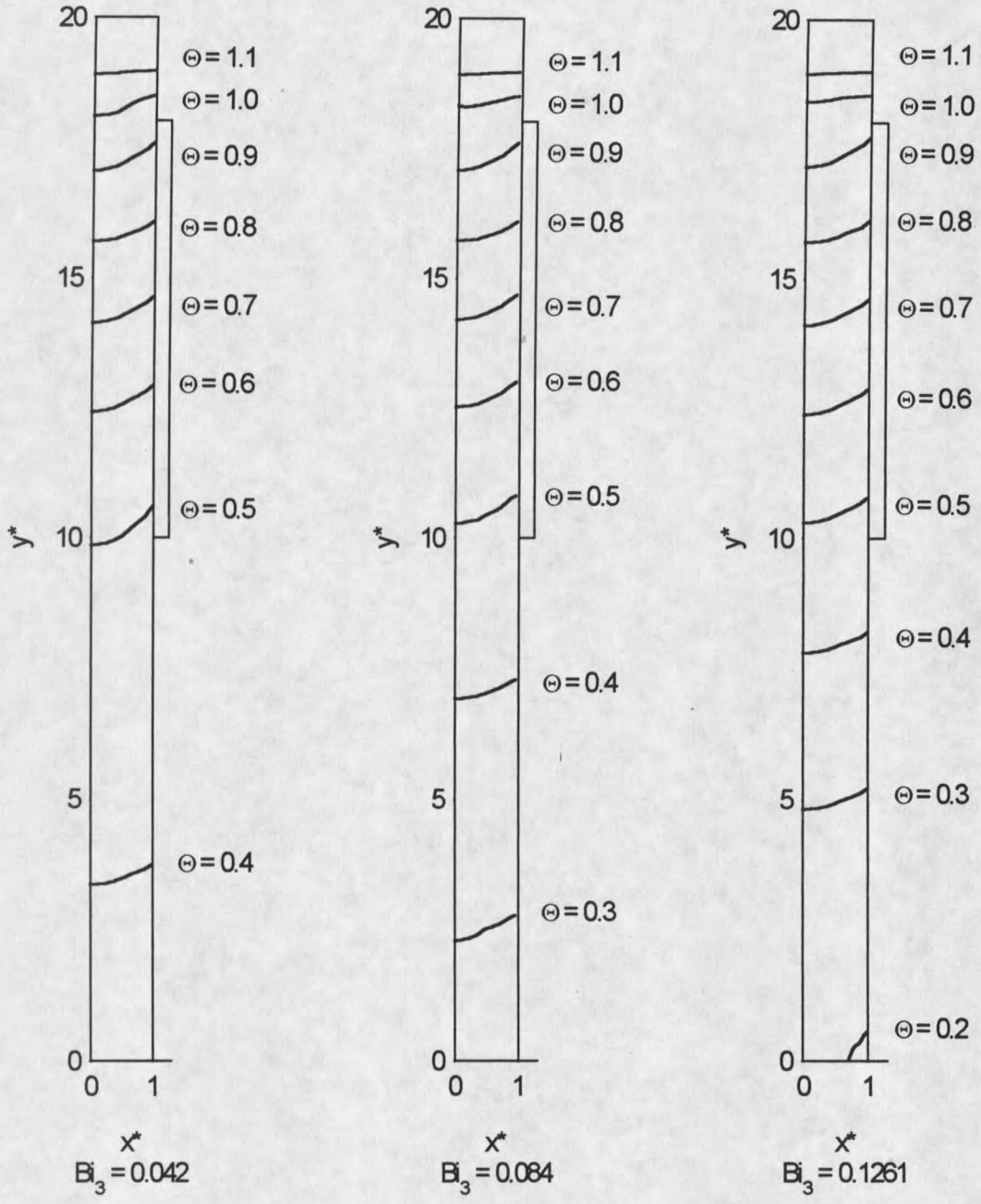

Figure 32 cont. Pe=1.2, Θ_0=1.2, Bi_2 = 0.0748

Figures 32 and 33 show the non-dimensional isotherms for Pe = 1.2 and 1.5 respectively. The superheat was $\Theta_0 = 1.2$ for these cases.

Figure 32 demonstrated that the effect of the post-mold cooling rate on the solidification front is not significant (locations of $\Theta = 1$). However, its effect on the post-mold temperature distribution is significant. For all three mold cooling rates presented here, that proved to be the case. Because the mold cooling rate influences the temperature distribution in the post-mold region, it was expected that the heat flux would be affected by the value of Bi_3.

The effect of the post-mold cooling rate was studied for another casting speed, Pe = 1.5, and Figure 33 shows the temperature distributions throughout the cast material for those conditions: Pe = 1.5; $\Theta_0 = 1.2$; Bi_2 = 0.0249,0.0499, 0.0748; Bi_3 = 0.042, 0.084, 0.126.

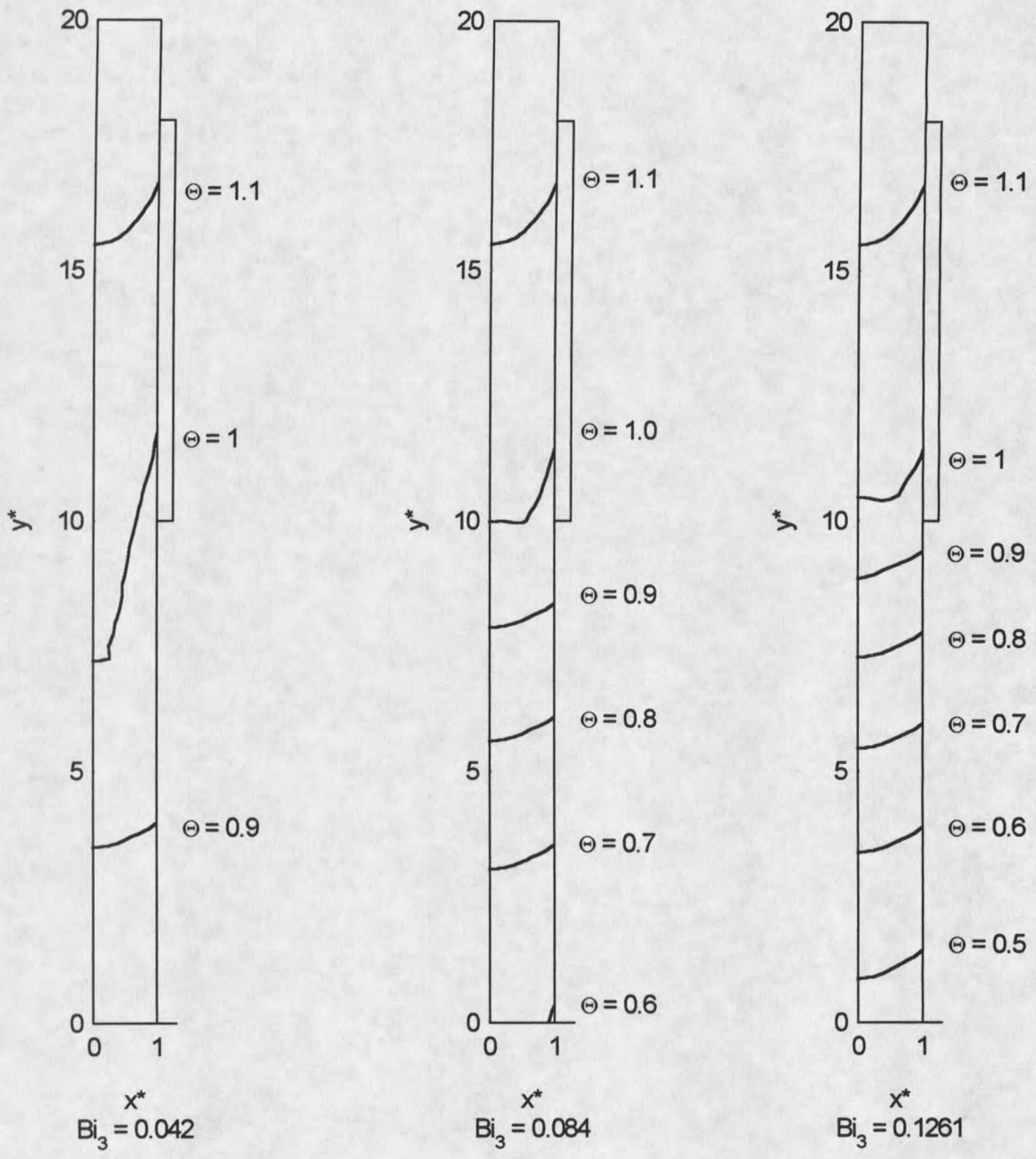

Figure 33. Effect of post-mold cooling rate on temperature distribution;

Pe = 1.5, Θ_0 = 1.2, Bi_2 = 0.0249, Bi_3 = 0.042, 0.084, 0.1261.

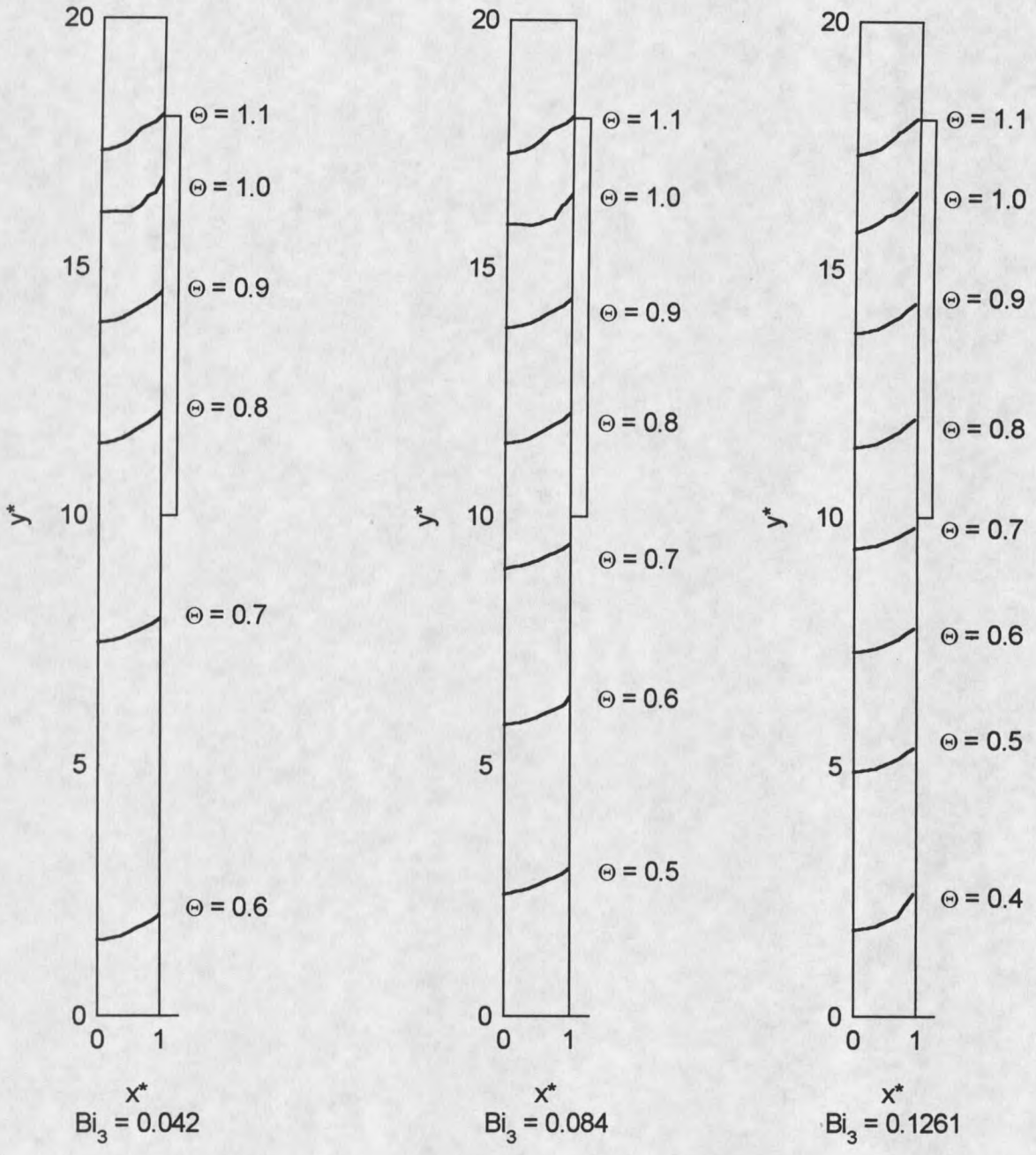

Figure 33 cont. Pe = 1.5, Θ_0 = 1.2, Bi_2 = 0.0499